

Unfolding force definition and the unified model for the mean unfolding force dependence on the loading rate

Rafayel Petrosyan*

Department of Physics, University of Alberta, Edmonton AB, T6G 2E1, Canada

Abstract

In single-molecule force spectroscopy experiments the mean unfolding force dependence on the loading rate is frequently used for obtaining information about the energetic and dynamic properties of the system under study. However, it is crucial to understand that different dynamic force spectroscopy (DFS) models are applicable in different regimes and that they might be using different definitions for the unfolding force. Here we discuss three definitions for the unfolding forces. We carried out Brownian dynamics simulations in order to demonstrate the difference between these definitions and compare DFS models. Importantly, we derive the mean unfolding force dependence for the whole range of the loading rates by unifying previously reported three DFS models. We have also obtained the exact result for the mean unfolding force dependence on the loading rate for the recently proposed heterogeneous DFS model.

* petrosyan@ualberta.ca
<https://orcid.org/0000-0003-1888-0379>

Introduction

In atomic force microscopy (AFM) based dynamic force spectroscopy (DFS) experiments the unfolding forces are being measured for a wide range of the loading rates. Afterward, the average unfolding force dependence on the loading rate from the appropriate DFS model is fitted to the corresponding data in order to gain information about the kinetic and energetic properties of the system (1–4). The system could be for example a protein or a ligand-receptor bond, but the theory is general and not limited to those. Hereafter we will be using the proteins terminology such as the native and unfolded states.

The first model that was proposed for analyzing DFS data was phenomenological model widely referred to as Bell-Evans model. It assumes first-order irreversible rate equation for the survival probability (5) with empirically determined exponentially force-dependent unfolding rate (6–8). Evans and Ritchie derive the unfolding force probability density function (PDF) and the most probable unfolding force depending on the loading rate and two parameters the unfolding rate and the distance between the native and the transition states. The mean unfolding force dependence on the loading rate for this model Eq. (1) was obtained later (9).

$$\langle F \rangle = \frac{k_B T}{x^\ddagger} e^{\frac{k_0 k_B T}{\dot{F} x^\ddagger}} E_1 \left(\frac{k_0 k_B T}{\dot{F} x^\ddagger} \right) \quad (1)$$

Where $\langle F \rangle$ is the mean unfolding force, k_B is the Boltzmann constant, T is the absolute temperature, x^\ddagger is the distance between the native and the transition states, k_0 is the unfolding rate in the absence of the external force, $\dot{F} \equiv dF/dt$ is the loading rate and $E_1(\)$ is the exponential integral (10, 11).

Here we would like to emphasize that the determination of the mean unfolding force from the experimentally obtained unfolding force distribution is less error-prone and more straightforward compared to the determination of the most probable unfolding force. The last is typically done by fitting a Gaussian to the unfolding force distribution (12, 13) neglecting the fact that generally the unfolding force distributions are asymmetric (14–18) and then taking the maximum of that fit as the most probable unfolding force.

The biomolecular (un)folding could be viewed as diffusion in the multidimensional potential energy surface. This means that each configuration of the biomolecule will be represented by a point in its degree of freedom space. For each configuration, there is also corresponding potential energy and the potential energy axes could be added as an additional dimension to the degree of freedom space. In that new space of degrees of freedom and the potential energy, we will have the abovementioned potential energy surface. In this framework, the continuous changes of the biomolecule configuration due to thermal motion could be viewed as Brownian motion of the particle in the degree of freedom space in the presence of the force (the gradient of the potential energy). Under certain assumptions, this multidimensional potential energy surface could be coarse-grained into a one-dimensional free energy profile (19). The use of Brownian dynamics (BD) simulations for mimicking dynamics of biomolecules is originating from these ideas. A simple scenario would be if one has smooth energy profile with a well and a barrier where particle is initially at the well (protein is folded at its native state) then due to Brownian motion particle might cross the barrier (protein unfolds), the determination of the rate of this reaction was addressed in the work of Kramers (20). He managed to solve the problem for large and small limiting cases of the viscosity (for biomolecular systems, generally, the limit of high viscosity is relevant) assuming that the barrier height is much larger than the thermal fluctuation energy ($k_B T$).

The Kramers result was used for the development of the next widely used DFS model the profile assumption model commonly referred to as Dudko-Hummer-Szabo model (15). Here two free energy profiles have been assumed: parabolic-cusp (14) and linear-cubic free energy profiles and the force-dependent unfolding rate was calculated based on Kramers result (20, 21). Again assuming first-order irreversible rate equation for the survival probability the approximate unfolding force PDF and the approximate mean unfolding force Eq. (2) (that was further improved (22) Eq. (3)) were derived for this model depending on the loading rate and three main parameters: the unfolding rate, the distance between the native state and the transition state and the free energy difference between the transition state and the native state. One of the important achievements of this study was that the authors managed to combine the results for two different free energy profiles into a single expression for the unfolding force PDF (and hence its moments). This raises the fourth parameter that specifies the free energy profile, it is equal to 1/2 for harmonic-cusp free energy profile, 2/3 for linear-cubic free energy profile and when it takes

value 1 the phenomenological model is recovered. Profile assumption model is applicable for the loading rates small enough so that the unfolding occurs before the Kramers high energy barrier approximation breaks down (20, 21).

$$\langle F \rangle \approx \frac{\Delta G^\ddagger}{\nu x^\ddagger} \left(1 - \left(\frac{k_B T}{\Delta G^\ddagger} \ln \left(\frac{k_0 k_B T e^{\frac{\Delta G^\ddagger}{k_B T} + \gamma}}{\dot{F} x^\ddagger} \right) \right)^\nu \right) \quad (2)$$

$$\langle F \rangle \approx \frac{\Delta G^\ddagger}{\nu x^\ddagger} \left(1 - \left(1 - \frac{k_B T}{\Delta G^\ddagger} e^{\frac{k_0 k_B T}{\dot{F} x^\ddagger}} E_1 \left(\frac{k_0 k_B T}{\dot{F} x^\ddagger} \right) \right)^\nu \right) \quad (3)$$

Where ΔG^\ddagger is the free energy difference between the transition and native states, ν is the free energy profile defining factor and $\gamma \approx 0.5772$ is the Euler-Masceroni constant.

The profile assumption model was further generalized for the case of a larger number of underlying free energy profiles (23). In this model the fourth parameter μ (similar to ν in the previous model (15)) determines the free energy profile, it assumes any value between 0 and 1. It gives the same results as the previous model (15) for values 1/2, 2/3 and 1. The mean unfolding force dependence on the loading rate for this model is given by Eq. (4).

$$\langle F \rangle \approx \frac{\Delta G^\ddagger}{\mu x^\ddagger} \left(1 - \left(\frac{k_B T}{\Delta G^\ddagger} \ln(\Lambda) \right) \right)^\mu \left(1 + \frac{\mu(3\mu - 2) \ln(\ln(\Lambda))}{\ln(\Lambda)} \right) \quad (4)$$

$$\text{Where } \Lambda \equiv \frac{k_0 k_B T \left(\frac{\Delta G^\ddagger}{k_B T} \right)^{2-3\mu} e^{\frac{\Delta G^\ddagger}{k_B T} + \gamma}}{x^\ddagger \dot{F}}.$$

A model that describes relatively well the unfolding force distributions for the low and high loading rates is commonly referred as Bullerjan-Sturm-Kroy model and here we will refer to it as a rapid model (18). Authors managed to calculate the PDF for the unfolding forces and mean unfolding force dependence on the loading rate Eq. (5). The last is simply the sum of the mean unfolding force predicted by the phenomenological model and the mean unfolding force for the limit of high loading rates when the unfolding is ballistic and follows the \sqrt{F} law (14).

$$\langle F \rangle \approx \frac{k_B T}{x^\ddagger} e^{\frac{k_0 k_B T}{F x^\ddagger}} E_1 \left(\frac{k_0 k_B T}{F x^\ddagger} \right) + \sqrt{2\zeta F x^\ddagger} \quad (5)$$

Where ζ quantifies the friction (that could be the combination of the solvent viscosity, internal friction due to interatomic interactions and other factors that are damping the fluctuations of the molecule (24) it is related to the diffusion coefficient as $\zeta = k_B T / D$). In this model harmonic-cusp free energy profile is assumed and using Kramers high friction approximation, the intrinsic

unfolding rate is expressed through other parameters of the system $k_0 = \frac{2\Delta G^\ddagger}{\zeta x^{\ddagger 2}} \sqrt{\frac{\Delta G^\ddagger}{\pi k_B T}} e^{-\frac{\Delta G^\ddagger}{k_B T}}$ (18).

In the close to equilibrium regime (for sufficiently low loading rates) system might hop back and forth between states before the final unfolding (25–31). All the above-discussed models neglect the possibility of refolding or use only the first unfolding force if hopping is observed. However, there is some information on the equilibrium properties of the system stored in the data obtained from close to equilibrium measurements that could give a more complete picture of the system under study.

A model that considers also the refolding rate in the rate equation for the survival probability is frequently referred as Friddle-Noy-De Yoreo model and we will refer to it as a reversible model (32–34). This model assumes exponentially force-dependent rates (6–8) as the phenomenological model (5) and considers that the force is applied on the system through the Hookean spring (henceforth spring). The mean unfolding force dependence on the loading rate Eq. (6) and on three parameters namely the unfolding rate, the distance between the native state and the transition state and the free energy difference between the unfolded and native states was obtained for this model (32–34).

$$\langle F \rangle \approx F_{\text{eq}} + \frac{k_B T}{x^\ddagger} e^{\frac{k(F_{\text{eq}})k_B T}{F x^\ddagger}} E_1 \left(\frac{k(F_{\text{eq}})k_B T}{F x^\ddagger} \right) \quad (6)$$

Where F_{eq} is the equilibrium force at which unfolding and refolding rates are having the same value (assuming that in the absence of force the unfolding rate is lower than the refolding rate), for this model $F_{\text{eq}} = \sqrt{2\kappa\Delta G}$ where κ is the spring constant, ΔG is the free energy difference

between unfolded and native states and $k(F_{\text{eq}}) = k_0 e^{\frac{F_{\text{eq}} x^\ddagger - \kappa x^{\ddagger 2}}{2 k_B T}}$. The unfolding force PDF of this model has not been reported yet. As emphasized in (34) the unfolding force here should be calculated from the total time (residence time or occupation time) spent in the native state before the final unfolding (loading rate multiplied by the residence time) that is the total force applied on native state while the system was in that state.

Some of the above-discussed models, that take only the first unfolding force, have been extended for the case when the force is applied through spring. For the phenomenological model when the force is applied through spring expression for the mean unfolding force Eq. (7) could

be obtained using the following rate expression $k(F) = k_0 e^{\frac{F x^\ddagger - \kappa x^{\ddagger 2}}{2 k_B T}}$.

$$\langle F \rangle = \frac{k_B T}{x^\ddagger} e^{\frac{k_0 k_B T e^{\frac{\kappa x^{\ddagger 2}}{2 k_B T}}}{F x^\ddagger}} E_1 \left(\frac{k_0 k_B T e^{\frac{\kappa x^{\ddagger 2}}{2 k_B T}}}{F x^\ddagger} \right) \quad (7)$$

For the profile assumption model in the case force is applied through the spring Eq. (8) is applicable (4, 35)(Maitra, Arya 2010, Arya 2016).

$$\langle F \rangle \approx \frac{\Delta G^\ddagger Z}{\nu x^\ddagger} \left(1 - \left(1 - \frac{k_B T}{\Delta G^\ddagger Z^3} e^{\frac{k_0 k_B T}{Z F x^\ddagger} e^{\frac{\Delta G^\ddagger}{k_B T} (1-Z^3)}} E_1 \left(\frac{k_0 k_B T}{F x^\ddagger} e^{\frac{\Delta G^\ddagger}{k_B T} (1-Z^3)} \right) \right)^\nu \right) \quad (8)$$

$$Z = 1 + \frac{\kappa}{\kappa_{G_0(x_{\min})}} \quad \text{and} \quad \kappa_{G_0(x_{\min})} \equiv \left. \frac{\partial^2 G_0(x)}{\partial x^2} \right|_{x=x_{\min}} \quad (9)$$

Where $\kappa_{G_0(x_{\min})}$ is the curvature of the molecular free energy profile at the native state as defined

in Eq. (9) and $G_0(x) = -\Delta G^\ddagger \frac{\nu}{1-\nu} \left(\frac{x}{x^\ddagger} \right)^{\frac{1}{1-\nu}} + \frac{\Delta G^\ddagger}{\nu} \frac{x}{x^\ddagger}$ is the model for the free energy profile (15).

For the rapid model, Eq. (10) was reported in the original study (18).

$$\langle F \rangle \approx \frac{k_B T}{Z x^\ddagger} e^{\frac{\sqrt{Z} k_{0un} k_B T e^{\frac{\Delta G^\ddagger}{k_B T} (1-Z)}}{F x^\ddagger}} E_1 \left(\sqrt{Z} \frac{k_{0un} k_B T e^{\frac{\Delta G^\ddagger}{k_B T} (1-Z)}}{F x^\ddagger} \right) + \sqrt{2\zeta F x^\ddagger} \quad (10)$$

This model assumes harmonic-cusp free energy profile hence using Eq. (9) $Z = 1 + \frac{\kappa x^\ddagger^2}{2\Delta G^\ddagger}$ can be obtained.

The main aim of this study is to show the importance of the definition of the unfolding force and compare the predictions of the mean unfolding force dependence on the loading rate from different DFS models. We also report for the first time the mean unfolding force dependence on the loading rate for the heterogeneous model (36) that assumes multiple native states. Finally we provide a new model (unified model) based on profile assumption (15, 22), reversible (33, 34) and rapid (14, 18) models that is applicable in the whole range of the loading rates from equilibrium to ballistic unfolding.

Results

Definition of the unfolding force

The determination of the unfolding force for the case of a single transition (Fig. 1) is straightforward. However, what should be taken as an unfolding force if the system hops back and forth between states before the final unfolding (Fig. 2)? For such situations we define three unfolding forces: first unfolding force is the product of the time at which the system visits the unfolded state for the first time and the loading rate, last unfolding force is the product of the time at which the system was in the native state for the last time and the loading rate, and reversible unfolding force is the product of the loading rate and the time that system spent on the native side of the transition state (Fig. 2 yellow stripes).

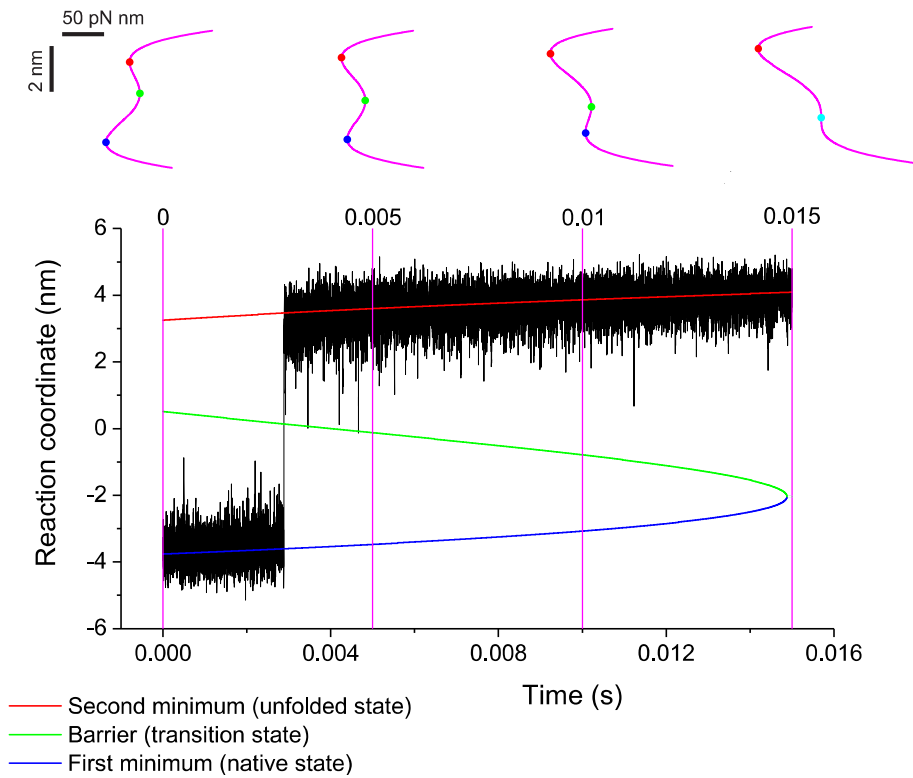


Figure 1. An example of a trajectory from BD simulation with a single transition. The quartic free energy profile that is under constantly increasing external force (with 1000 pN/s loading rate) was used. There is a single transition here and hence no ambiguity in the determination of the unfolding force. The graphs of the free energy profile on top are given at different times (0.005 seconds apart) showing that the first minimum (blue dot) and the maximum (green dot) getting closer with time and eventually merging (cyan dot). The blue, green and red lines are showing the positions of the first minimum, maximum, and second minimum respectively as functions of time.

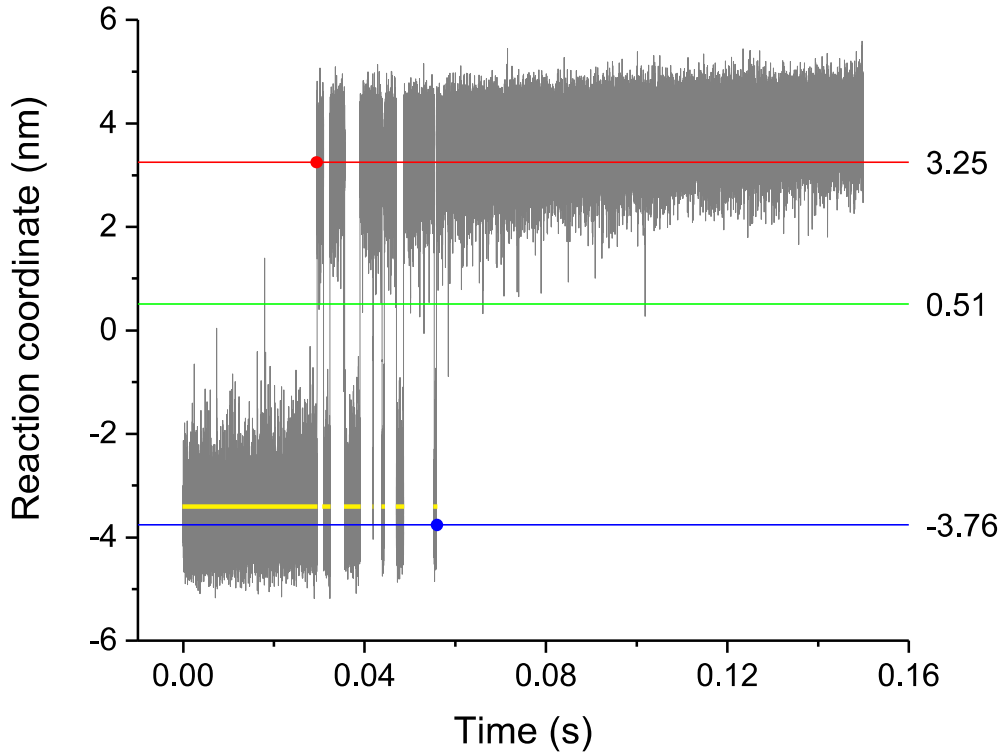


Figure 2. An example of a trajectory from BD simulation with multiple transitions between native and unfolded states. The quartic free energy profile that is under constantly increasing external force (with 100 pN/s loading rate) was used. We define three unfolding forces: first unfolding force is the product of the time at which system visits the unfolded state ($x = 3.25$ nm) for the first time (red dot) and the loading rate, last unfolding force is the product of the time at which the system was in the native state ($x = -3.76$ nm) for the last time (blue dot) and the loading rate, and reversible unfolding force is the product of the loading rate and the time that system spent on the native side of the transition state (time spent below the green line $x < 0.51$ nm, yellow strip). The blue, green and red lines, in this case, are showing the positions of the first minimum (native state), maximum (transition state), and second minimum (unfolded state) in the absence of the external force. If we refer to the native, transition and unfolded states in the definitions of the unfolding forces always their reaction coordinate values in the absence of force are meant.

As can be seen from Fig. 1 the positions of the extremes of the free energy profile change with time if external time dependent force is applied. However, when we refer to the native, transition and unfolded states in the unfolding force definitions we mean their reaction coordinate values in the absence of the external force. Because when the force builds up, for example, the protein structure will change and that structure can be very different from the native structure.

In order to see how the means of these three unfolding forces depend on the loading rate, we carried out BD simulations using quartic free energy profile under an external force that

increases with a constant loading rate. We generated 3000 trajectories for each loading rate, for the loading rates ranging 12 orders of magnitude Fig. 3 (see methods section for more details).

The surprising observation is that the mean last unfolding force shows non-monotonic dependence on the loading rate. At low enough loading rates it starts to increase with the decrease of the loading rate, a phenomenon that was not observed previously. This means that the time when the system was in the native state for the last time increases faster than the loading rate decreases so that their product increases. The behavior of the mean last unfolding force at even lower loading rates will be discussed at the end of this section (Fig. 7). The mean reversible unfolding force at low loading rate regime with the decrease of the loading rate tends to a constant value of F_{eq} . This means that the mean time spent below the transition state increases with the same amount as the loading rate decreases. The decrease in the mean first unfolding force at low loading rate regime is evident. Recall that the first unfolding force is the time when the first unfolding occurred multiplied by the loading rate. In the absence of the external force, there is a constant mean time of the system to visit the unfolded state for the first time (mean first passage time). In the presence of slowly changing external force, the time when the first unfolding occurred tends to that constant, i.e. one term in the product tends to constant while the other decreases, hence the decrease of the first unfolding force with decreasing loading rate.

As can be seen from Fig. 3 three differently defined mean unfolding forces converge with the increase of the loading rate. This is the result of moving away from equilibrium and the evidence of the regime where there are mostly single transitions in trajectories. In the case of a single transition, the difference between three unfolding forces is negligible as long as the time spent during the transition (transition path time) is negligible compared to the time spent before the transition (residence time of the native state). This is true for low loading rates for which also the hopping is common. For very high loading rates this is not true and we show only mean reversible unfolding force considering that in the vast majority of trajectories there is only a single transition, and for single transition the determination of the unfolding force is straightforward.

Next observation that can be noticed from Fig. 3B is the kink around 10^6 to 10^7 pN/s of the loading rate value. After this critical value of the loading rate, the data points lay on a line with a higher slope. This is the indication of the change in the regime of unfolding. At such high loading rates, the unfolding mostly occurs after the disappearance of the barrier.

Hereby we have specified three regimes, low loading rate regime (close to equilibrium), intermediate loading rate regime (non-equilibrium), and high loading rate regime (non-equilibrium, ballistic unfolding). The smoothness of kinks between regimes in the mean unfolding force dependence on the loading rate graphs is due to the fact that the mean unfolding force for the given loading rate contains data from many trajectories that can show multiple transitions between states, single transition or a transition to the unfolded state after the barrier disappeared.

A unified model for the mean unfolding force dependence on the loading rate

For accurately predicting the behavior of the mean unfolding force dependence on the loading rate in all three regimes we developed a unified model. We used the force-dependent unfolding rate expression proposed by (15) and calculated mean first unfolding force for the low and intermediate loading rates following the method proposed by (22). Next, we extended that result for the case of high loading rates when the unfolding is happening after the disappearance of the barrier (14, 18) which results in Eq. (11). Derivations can be found in Appendix A.

$$\begin{aligned} \langle F_{\text{First}} \rangle \approx & \frac{\Delta G^\ddagger}{\nu x^\ddagger} \left(1 - \left| 1 - \frac{k_B T}{\Delta G^\ddagger} e^{\frac{k_0 k_B T}{x^\ddagger \dot{F}}} E_1 \left(\frac{k_0 k_B T}{x^\ddagger \dot{F}} \right) \right|^\nu \right) \cdot \theta \left(\dot{F}_{\text{cFirst}} - \dot{F} \right) + \\ & \left(\frac{\Delta G^\ddagger}{\nu x^\ddagger} - \sqrt{2 \dot{F}_{\text{cFirst}} x^\ddagger \zeta} + \sqrt{2 \dot{F} x^\ddagger \zeta} \right) \cdot \theta \left(\dot{F} - \dot{F}_{\text{cFirst}} \right) \end{aligned} \quad (11)$$

Where $\dot{F}_{\text{cFirst}} = \frac{k_0 k_B T e^{\frac{\Delta G^\ddagger}{k_B T} + \gamma}}{x^\ddagger} \left(1 - e^{-\frac{\Delta G^\ddagger}{k_B T}} \right)$, k_0 is not an independent parameter, it can be calculated

using the Kramers approximation if the free energy profile is known, for example for the linear-

cubic profile ($\nu = 2/3$), we will have $k_0 = \frac{3 \Delta G^\ddagger}{\pi \zeta x^{\ddagger 2}} e^{-\frac{\Delta G^\ddagger}{k_B T}}$ in contrast to Eq. (5) where the harmonic-

cus profile is assumed. Generally using linear-cubic free energy profile is more adequate as discussed in (15, 35), and we will assume that profile in the future i.e. $\nu = 2/3$ if not specified.

Here $\theta(\)$ is the Heaviside step function $\theta(x) = \begin{cases} 1, & x > 0 \\ 0, & x \leq 0 \end{cases}$. Hereby mean first unfolding force

dependence on the loading rate is determined by 3 independent parameters (x^\ddagger , ΔG^\ddagger and ζ).

Following the same procedure except this time calculating mean differently (33) we obtained (see Appendix A for details) mean reversible unfolding force Eq. (12).

$$\langle F_{\text{Rev}} \rangle \approx \frac{\Delta G^\ddagger}{\nu x^\ddagger} \left(1 - \left| \left(1 - \frac{\nu F_{\text{eq}} x^\ddagger}{\Delta G^\ddagger} \right)^{\frac{1}{\nu}} - \frac{k_B T}{\Delta G^\ddagger} e^{\frac{k_0 k_B T}{x^\ddagger \dot{F}}} e^{\frac{\Delta G^\ddagger}{k_B T} \left(1 - \left(1 - \frac{\nu F_{\text{eq}} x^\ddagger}{\Delta G^\ddagger} \right)^{\frac{1}{\nu}} \right)} \right| \left| E_1 \left(\frac{k_0 k_B T}{x^\ddagger \dot{F}} e^{\frac{\Delta G^\ddagger}{k_B T} \left(1 - \left(1 - \frac{\nu F_{\text{eq}} x^\ddagger}{\Delta G^\ddagger} \right)^{\frac{1}{\nu}} \right)} \right) \right| \right)^{\nu}. \quad (12)$$

$$\theta \left(\dot{F}_{\text{cRev}} - \dot{F} \right) + \left(\frac{\Delta G^\ddagger}{\nu x^\ddagger} - \sqrt{2 \dot{F}_{\text{cRev}} x^\ddagger \zeta} + \sqrt{2 \dot{F} x^\ddagger \zeta} \right) \cdot \theta \left(\dot{F} - \dot{F}_{\text{cRev}} \right)$$

$$\text{Where } \dot{F}_{\text{cRev}} = \frac{k_0 k_B T e^{\frac{\Delta G^\ddagger}{k_B T} + \gamma}}{x^\ddagger} \left(1 - e^{-\frac{\Delta G^\ddagger}{k_B T} \left(1 - \left(1 - \frac{\nu F_{\text{eq}} x^\ddagger}{\Delta G^\ddagger} \right)^{\frac{1}{\nu}} \right)} \right). \text{ Hereby mean reversible unfolding force}$$

dependence on the loading rate is determined by 4 independent parameters (x^\ddagger , ΔG^\ddagger , F_{eq} and ζ).

Notice that the critical loading rate is depending on the unfolding force definition. Generally, mean reversible unfolding force riches the given force at the lower loading rate than the mean first unfolding force since by definition for the same trajectory the first unfolding force is not higher than the reversible unfolding force. With the increase of the loading rate, the number of trajectories with hopping decreases and due to this the first and reversible mean unfolding forces are getting closer, but eventually the mean reversible unfolding force riches the critical force at a slightly smaller loading rate than the mean first unfolding force.

The determination of the mean last unfolding force can be done based on the symmetry arguments. We observe from Fig. 2 that $\langle F_{\text{Last}} \rangle = \langle F_{\text{Rev}} \rangle + \langle F_x \rangle$ where $\langle F_x \rangle$ is the mean force due to time spent in the unfolded state side of the barrier (above 0.51 nm) before the last unfolding. $\langle F_x \rangle$ equals to the time spent in the unfolded state before the last unfolding multiplied by the

loading rate. Interestingly, it is possible to calculate $\langle F_x \rangle$ from the refolding protocol, namely, $\langle F_x \rangle \approx \langle F_{\text{FirstRef}} \rangle - \langle F_{\text{RevRef}} \rangle$ where $\langle F_{\text{FirstRef}} \rangle$ is the mean first refolding force and $\langle F_{\text{RevRef}} \rangle$ is the mean reversible refolding force. Hence the mean last unfolding force can be calculated by Eq. (13).

$$\langle F_{\text{Last}} \rangle \approx \langle F_{\text{Rev}} \rangle + \langle F_{\text{FirstRef}} \rangle - \langle F_{\text{RevRef}} \rangle \quad (13)$$

Where $\langle F_{\text{FirstRef}} \rangle$ and $\langle F_{\text{RevRef}} \rangle$ can be calculated following the same path as for $\langle F_{\text{First}} \rangle$ and $\langle F_{\text{Rev}} \rangle$ only using force dependant refolding rate as in (37) and different integration limits (see Appendix A for details), which results in Eq. (14) and Eq. (15).

$$\langle F_{\text{FirstRef}} \rangle \approx \frac{\Delta G_{\text{ref}}^\ddagger}{\nu x_{\text{ref}}^\ddagger} \left[\left(\left(1 + \frac{\nu F_{\text{fin}} x_{\text{ref}}^\ddagger}{\Delta G_{\text{ref}}^\ddagger} \right)^{\frac{1}{\nu}} - \frac{k_{\text{B}} T}{\Delta G_{\text{ref}}^\ddagger} e^{\frac{k_{0\text{ref}} k_{\text{B}} T}{x_{\text{ref}}^\ddagger \dot{F}}} e^{\frac{\Delta G_{\text{ref}}^\ddagger}{k_{\text{B}} T} \left(1 - \left(1 + \frac{\nu F_{\text{fin}} x_{\text{ref}}^\ddagger}{\Delta G_{\text{ref}}^\ddagger} \right)^{\frac{1}{\nu}} \right)} \right) E_1 \left(\frac{k_{0\text{ref}} k_{\text{B}} T}{x_{\text{ref}}^\ddagger \dot{F}} e^{\frac{\Delta G_{\text{ref}}^\ddagger}{k_{\text{B}} T} \left(1 - \left(1 + \frac{\nu F_{\text{fin}} x_{\text{ref}}^\ddagger}{\Delta G_{\text{ref}}^\ddagger} \right)^{\frac{1}{\nu}} \right)} \right) \right] - 1 \right] \cdot \theta \left(\dot{F}_{\text{cFirstRef}} - \dot{F} \right) + \left(-\frac{\Delta G_{\text{ref}}^\ddagger}{\nu x_{\text{ref}}^\ddagger} + \sqrt{2 \dot{F}_{\text{cFirstRef}} x_{\text{ref}}^\ddagger \zeta} - \sqrt{2 \dot{F} x_{\text{ref}}^\ddagger \zeta} \right) \cdot \theta \left(\dot{F} - \dot{F}_{\text{cFirstRef}} \right) \quad (14)$$

Where $\dot{F}_{\text{cFirstRef}} = \frac{k_{0\text{ref}} k_{\text{B}} T e^{\frac{\Delta G_{\text{ref}}^\ddagger}{k_{\text{B}} T} + \gamma}}{x_{\text{ref}}^\ddagger} \left(1 - e^{-\frac{\Delta G_{\text{ref}}^\ddagger}{k_{\text{B}} T} \left(1 + \frac{\nu F_{\text{fin}} x_{\text{ref}}^\ddagger}{\Delta G_{\text{ref}}^\ddagger} \right)^{\frac{1}{\nu}}} \right)$, $k_{0\text{ref}} = \frac{3 \Delta G_{\text{ref}}^\ddagger}{\pi \zeta x_{\text{ref}}^\ddagger} e^{-\frac{\Delta G_{\text{ref}}^\ddagger}{k_{\text{B}} T}}$ and F_{fin} is the final

force, that is the force till which the system is pulled and from where the (hypothetical) refolding protocol starts. The final force is set by the experimental design and is not an intrinsic parameter describing the system.

$$\langle F_{\text{RevRef}} \rangle \approx \frac{\Delta G_{\text{ref}}^\ddagger}{\nu x_{\text{ref}}^\ddagger} \left(\left(1 + \frac{\nu F_{\text{eq}} x_{\text{ref}}^\ddagger}{\Delta G_{\text{ref}}^\ddagger} \right)^{\frac{1}{\nu}} - \frac{k_{\text{B}} T}{\Delta G_{\text{ref}}^\ddagger} e^{\frac{k_{0\text{ref}} k_{\text{B}} T}{x_{\text{ref}}^\ddagger F}} e^{\frac{\Delta G_{\text{ref}}^\ddagger}{k_{\text{B}} T} \left(1 - \left(1 + \frac{\nu F_{\text{eq}} x_{\text{ref}}^\ddagger}{\Delta G_{\text{ref}}^\ddagger} \right)^{\frac{1}{\nu}} \right)} \right) E_1 \left(\frac{k_{0\text{ref}} k_{\text{B}} T}{x_{\text{ref}}^\ddagger F} e^{\frac{\Delta G_{\text{ref}}^\ddagger}{k_{\text{B}} T} \left(1 - \left(1 + \frac{\nu F_{\text{eq}} x_{\text{ref}}^\ddagger}{\Delta G_{\text{ref}}^\ddagger} \right)^{\frac{1}{\nu}} \right)} \right) - 1 \right) \cdot \theta \left(F_{\text{cRevRef}} - F \right) + \left(-\frac{\Delta G_{\text{ref}}^\ddagger}{\nu x_{\text{ref}}^\ddagger} + \sqrt{2 F_{\text{cRevRef}} x_{\text{ref}}^\ddagger \zeta} - \sqrt{2 F x_{\text{ref}}^\ddagger \zeta} \right) \cdot \theta \left(F - F_{\text{cRevRef}} \right) \quad (15)$$

Where $F_{\text{cRevRef}} = \frac{k_{0\text{ref}} k_{\text{B}} T e^{\frac{\Delta G_{\text{ref}}^\ddagger + \gamma}{k_{\text{B}} T}}}{x_{\text{ref}}^\ddagger} \left(1 - e^{-\frac{\Delta G_{\text{ref}}^\ddagger}{k_{\text{B}} T} \left(1 + \frac{\nu F_{\text{eq}} x_{\text{ref}}^\ddagger}{\Delta G_{\text{ref}}^\ddagger} \right)^{\frac{1}{\nu}}} \right)$. F_{eq} in this case is also not an

independent parameter, since in Eq.(14) and Eq. (15) there are parameters involved in describing the refolding portion of the free energy profile. The equilibrium unfolding force can be calculated using the probability of finding the system folded at a given force (34)

$$F_{\text{eq}} = \int_0^\infty \frac{1}{1 + e^{\frac{F(x^\ddagger + x_{\text{ref}}^\ddagger) - (\Delta G^\ddagger - \Delta G_{\text{ref}}^\ddagger)}{k_{\text{B}} T}}} = \frac{k_{\text{B}} T}{x^\ddagger + x_{\text{ref}}^\ddagger} \ln \left(1 + e^{\frac{\Delta G^\ddagger - \Delta G_{\text{ref}}^\ddagger}{k_{\text{B}} T}} \right). \text{ This estimation of } F_{\text{eq}} \text{ is model}$$

independent in the sense that we did not assume force dependent unfolding and refolding rates such as phenomenological (6–8) or profile assumption (15, 37) which then could be solved to find F_{eq} (33, 34). By plugging in Eq. (12), Eq. (14) and Eq. (15) into Eq. (13) the mean last unfolding force dependence on the loading rate is determined by 5 independent parameters (x^\ddagger , ΔG^\ddagger , x_{ref}^\ddagger , $\Delta G_{\text{ref}}^\ddagger$ and ζ). Independently of using refolding protocol Eq. (13) with Eq. (12), Eq. (14) and Eq. (15) is applicable for predicting the mean last unfolding force dependence on the loading rate.

We would like also to mention that exponential integral and Heaviside step function can be approximated using other well-known functions $e^x E_1(x) \approx \ln \left(1 + \frac{e^{-x}}{x} \right)$ and $\theta(x) \approx \frac{1}{1 + e^{-qx}}$ where q is a large positive number (11). However, we provide the fitting function files (avoiding these approximations) that can be used for data analyses (Supplementary Information).

Comparing models predictions to simulated data

For showing how well do models predict mean unfolding force dependence on the loading rate we plot models predictions and the data from the BD simulations on the same graph Fig. 3. The parameters for plotting the models were the same as in the BD simulations. Further to quantify how well do models predict BD simulation data we have calculated R^2 and χ^2 (see methods section for details) in Table 1.

We observe that the phenomenological model (5, 9) fails at high and intermediate loading rates. The main disadvantage of the profile assumption models (15, 22, 23) is that they fail at high loading rates. Although an *ad hoc* sum of the phenomenological (9) and the high loading rate result (14, 18) the rapid model (18) gives arguably the best prediction among previously proposed models. This could be because the intermediate loading rate regime range is small compared to the high loading rate regime and we generated more data in the high loading rate regime through BD simulations. The loading rate range for the BD simulations was chosen based on previous experimental and molecular dynamics simulations studies (13). The unified model clearly gives the overall best prediction and in addition it also applicable for the mean reversible and last unfolding forces. According to our model the mean last unfolding force tends to a constant at lower loading rates as it will be revealed later (Fig. 7), however, conducting simulations at such low loading rates is challenging due to long simulation times and large memory required to deal with simulated data. Hence, the prediction of the unified last model at low loading rates needs further verification.

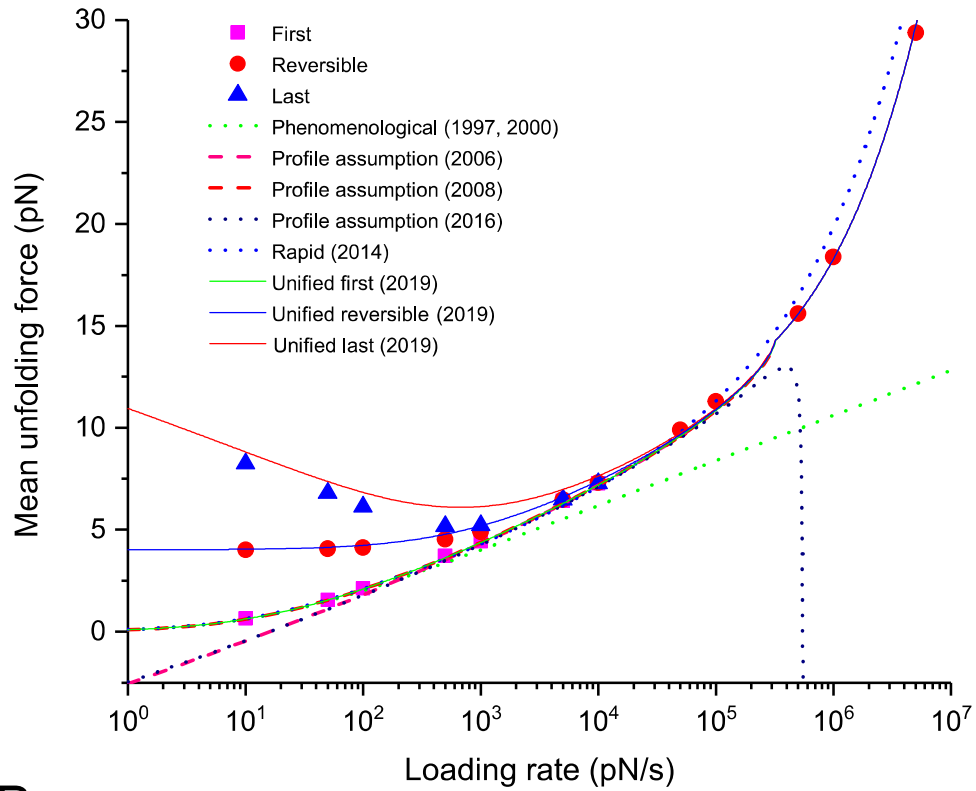
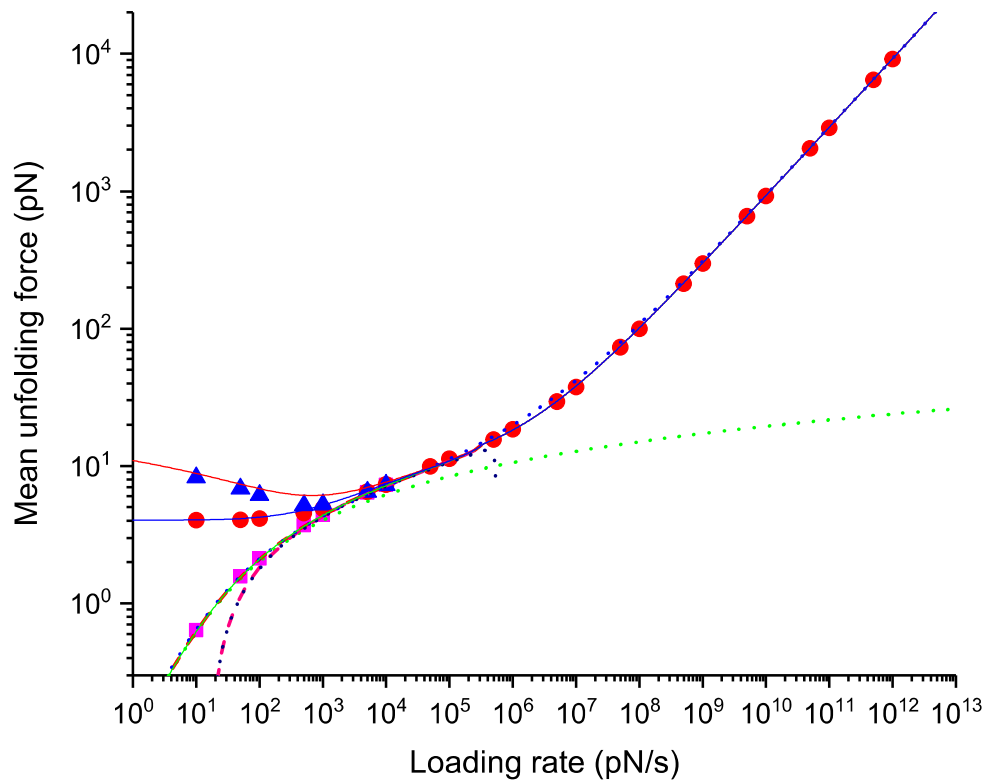
A**B**

Figure 3. Mean unfolding force dependence on the loading rate from BD simulations with quartic free energy profile and the predictions from the DFS models. (B) shows the log-log plot for the data as in (A) but for the larger range of the loading rates. Three regimes can be distinguished from (B). Low loading rate regime is where three differently defined mean unfolding forces diverge, this regime ends roughly where the mean last unfolding force has a minimum, the mean reversible unfolding force rises from the constant F_{eq} value and the mean first unfolding force follows a different slope, around 1000 pN/s. The intermediate loading rate regime starts where the low loading rate regime ends and ends roughly where the change in the slope can be noticed around 10^6 pN/s, indicating that unfolding occurs after the barrier is disappeared. The models are plotted using the parameters from the BD simulation (hence these are NOT fits). Phenomenological (1997, 2000) represents Eq. (1), profile assumption (2006) represents Eq. (2), profile assumption (2008) represents Eq. (3), profile assumption (2016) represents Eq. (4), rapid (2014) represents Eq. (5), unified first (2019) represents Eq. (11), unified reversible (2019) represents Eq. (12), unified last (2019) represents Eq. (13) where Eq. (12), Eq. (14) and Eq. (15) were used. Table 1 shows how well models predict the data from this figure. The parameters used in models were $k_B T = 4.1$ pN nm, $x^\ddagger = 4.27$ nm, $k_0 = 9.33$ s⁻¹, $\Delta G^\ddagger = 40.62$ pN nm, $\zeta = 10^{-5}$ pN s/nm, $F_{eq} = 4.02$ pN, $F_{fin} = 15$ pN, $v = 0.66667$, $\mu = 0.5872$, $x_{ref}^\ddagger = 2.74$ nm, $k_{0ref} = 6495$ s⁻¹, $\Delta G_{ref}^\ddagger = 12.41$ pN nm. The error bars for the standard error of the mean are smaller than the symbols.

Model	Low loading rates ($\dot{F} < 5000$ pN/s)		Intermediate loading rates (5000 pN/s $\leq \dot{F} \leq 10^6$ pN/s)		High loading rates ($\dot{F} > 10^6$ pN/s)		All loading rates	
	R ²	χ^2	R ²	χ^2	R ²	χ^2	R ²	χ^2
Phenomenological (1997)	0.9695	0.1809	0.0275	12.6468	-0.4443	1882.94	-0.1878	1895.77
Profile assumption (2006)	0.8446	6.3365	1.0414- 0.1402i	-0.432+ 1.4711i	-0.4441 -0.0072i	1836.41+ 88.0905i	-0.1876- 0.0059i	1842.31+ 89.5616i
Profile assumption (2008)	0.9889	0.2245	1.0415- 0.1402i	-0.4327+ 1.4711i	-0.4441 -0.0072i	1836.41+ 88.0905i	-0.1876- 0.0059i	1836.2+ 89.5616i
Profile assumption (2016)	0.842	6.2111	0.883+ 0.028i	1.598- 0.2846i	-0.4446 -0.0088i	1824.61+ 107.478i	-0.188- 0.0073i	1832.42+ 107.193i
Rapid (2014)	0.9968	0.0187	0.9727	0.3191	0.9997	4.145	0.9997	4.4828
Unified first (2019)	0.9987	0.0093	0.997	0.0693	0.9998	0.4946	0.9998	0.5732
Unified reversible (2019)	0.6972	0.5088	0.9977	0.0553	0.9998	0.4961	0.9998	1.0602
Unified last (2019)	0.5613	2.2316	0.9952	0.1886	0.9998	0.4974	0.9998	2.9176

Table 1. For quantifying how well models predict the simulated data we calculated R^2 and χ^2 (see methods section) for each model plotted in Fig. 3 at three regimes separately and then all together (last column). Some of the models predict complex values for the mean unfolding force at high loading rates, we present R^2 and χ^2 for these once too for the completeness. Perfect prediction would result in $R^2 = 1$ and $\chi^2 = 0$.

Mean first unfolding force dependence on the loading rate for the heterogeneous model

Heterogeneous model (36) assumes that the native state is not necessarily a single well-defined state with a single minimum in the energy landscape, but an ensemble of such states which have different unfolding rates and the interconversion rate between these native states is small compared to the unfolding rates. For such heterogeneous adiabatic model authors assumed first-order irreversible rate equation for the survival probability and exponentially force-dependent unfolding rate (6–8) that was also used in the phenomenological model (5) and managed to derive the unfolding force PDF that depends on 3 parameters, the heterogeneity, the ensemble averaged unfolding rate and the ensemble averaged distance between the native and the transition states (36).

We report for the first time the mean first unfolding force dependence on the loading rate for this model that was calculated exactly using unfolding force PDF (see Appendix B for details).

$$\langle F_{\text{First}} \rangle = \frac{k_{\text{B}}TH}{x^\ddagger} \left(\frac{k_0 k_{\text{B}}TH}{F x^\ddagger} \right)^{-\frac{1}{H}} {}_2F_1 \left(\frac{1}{H}, \frac{1}{H}; 1 + \frac{1}{H}; 1 - \frac{F x^\ddagger}{k_0 k_{\text{B}}TH} \right) \quad (16)$$

Where x^\ddagger is the ensemble averaged distance between the native states and the transition state, k_0 is the ensemble averaged unfolding rate, H is a measure of the overall scale of heterogeneity, and ${}_2F_1$ is the hypergeometric function (10, 11). In Fig. 4 we plot Eq. (16) for the different values of heterogeneity – H . We observe that the mean unfolding force increases with the increase of H and in the limit $H \rightarrow 0$ the phenomenological model prediction Eq. (1) is recovered. Since there is no heterogeneity in our BD simulations the heterogeneous model would be in an unfavorable position for predicting the data and would have reduced to the phenomenological model, hence we do not include this model in our analyses. We also show in Appendix B how the heterogeneous model could be incorporated into the unified model.

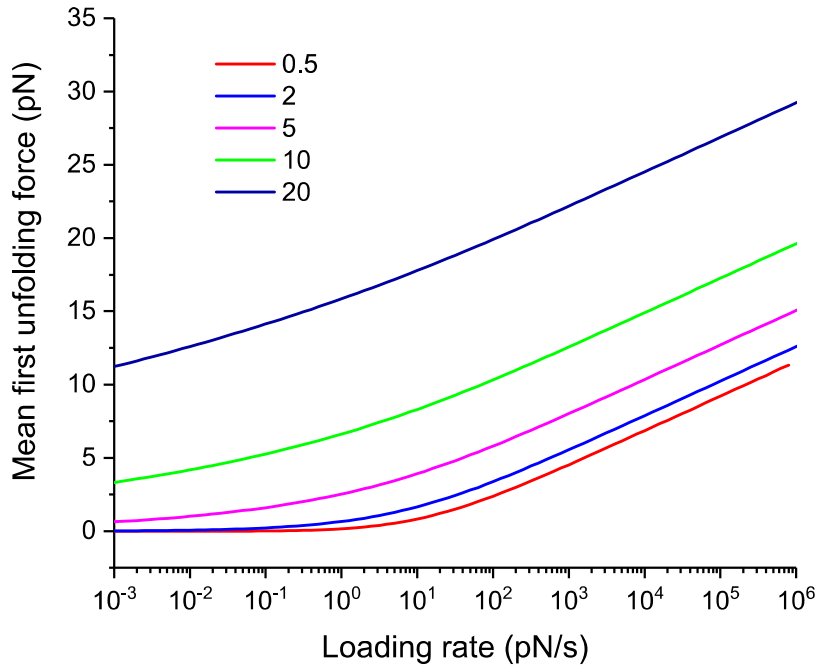


Figure 4. Prediction of the mean first unfolding force dependence on the loading rate for the heterogeneous model (Hinzevsky, Heyon Thirumalai 2016) for different values of heterogeneity – H . Parameters used in Eq. (16) were $k_B T = 4.1 \text{ pN nm}$, $x^\ddagger = 4 \text{ nm}$ and $k_0 = 9 \text{ s}^{-1}$. For $H \rightarrow 0$ the phenomenological model behavior Eq. (1) is recovered. Higher heterogeneity causes higher mean unfolding force.

Unified model when force is applied through spring

We have further extended the unified model for the case when the system is being pulled through spring. The mean unfolding forces dependences on the loading rates were derived using the same methods as when force was applied directly, the only difference is that for this case different force dependant unfolding and refolding rates were used (see Appendix C for derivation) (35). Our calculations result in Eq. (17), Eq. (18), Eq. (19) and Eq. (20) for the mean first unfolding force, mean reversible unfolding force, mean first refolding force and mean reversible refolding force respectively. The last three are used for calculating the mean last unfolding force by Eq. (13).

$$\langle F_{\text{First}} \rangle \approx \frac{\Delta G^\ddagger}{\nu x^\ddagger Z} \left(Z^2 - \left| Z^{\frac{2}{\nu}} - \frac{k_B T}{\Delta G^\ddagger} e^{\frac{k_0 k_B T}{x^\ddagger \dot{F} Z}} e^{\frac{\Delta G^\ddagger}{k_B T} \left(1 - Z^{\frac{2}{\nu}} \right)} \right| E_1 \left(\frac{k_0 k_B T}{x^\ddagger \dot{F} Z} e^{\frac{\Delta G^\ddagger}{k_B T} \left(1 - Z^{\frac{2}{\nu}} \right)} \right) \right)^{\nu} \cdot \theta \left(\dot{F}_{\text{cFirst}} - \dot{F} \right) + \quad (17)$$

$$\left(\frac{\Delta G^\ddagger Z}{\nu x^\ddagger} - \sqrt{2 \dot{F}_{\text{cFirst}} x^\ddagger \zeta} + \sqrt{2 \dot{F} x^\ddagger \zeta} \right) \cdot \theta \left(\dot{F} - \dot{F}_{\text{cFirst}} \right)$$

Where $\dot{F}_{\text{cFirst}} = \frac{k_0 k_B T e^{\frac{\Delta G^\ddagger}{k_B T} + \gamma}}{x^\ddagger Z} \left(1 - e^{-\frac{\Delta G^\ddagger Z^{\frac{2}{\nu}}}{k_B T}} \right)$ and Z is given by Eq. (9), which for linear-cubic free

energy profile reduce to $Z = 1 + \frac{\kappa \nu^{\frac{2}{3}}}{6 \Delta G^\ddagger}$.

$$\langle F_{\text{Rev}} \rangle \approx \frac{\Delta G^\ddagger}{\nu x^\ddagger Z} \left(Z^2 - \left(Z^2 - \frac{\nu F_{\text{eq}} x^\ddagger Z}{\Delta G^\ddagger} \right)^{\frac{1}{\nu}} - \frac{k_B T}{\Delta G^\ddagger} e^{\frac{k_0 k_B T}{x^\ddagger \dot{F} Z}} e^{\frac{\Delta G^\ddagger}{k_B T} \left(1 - \left(Z^2 - \frac{\nu F_{\text{eq}} x^\ddagger Z}{\Delta G^\ddagger} \right)^{\frac{1}{\nu}} \right)} \right)^{\nu} E_1 \left(\frac{k_0 k_B T}{x^\ddagger \dot{F} Z} e^{\frac{\Delta G^\ddagger}{k_B T} \left(1 - \left(Z^2 - \frac{\nu F_{\text{eq}} x^\ddagger Z}{\Delta G^\ddagger} \right)^{\frac{1}{\nu}} \right)} \right)^{\nu} \cdot \theta \left(\dot{F}_{\text{cRev}} - \dot{F} \right) + \left(\frac{\Delta G^\ddagger Z}{\nu x^\ddagger} - \sqrt{2 \dot{F}_{\text{cRev}} x^\ddagger \zeta} + \sqrt{2 \dot{F} x^\ddagger \zeta} \right) \cdot \theta \left(\dot{F} - \dot{F}_{\text{cRev}} \right) \quad (18)$$

$$\text{Where } \dot{F}_{\text{cRev}} = \frac{k_0 k_B T e^{\frac{\Delta G^\ddagger}{k_B T} + \gamma}}{x^\ddagger Z} \left(1 - e^{-\frac{\Delta G^\ddagger}{k_B T} \left(Z^2 - \frac{\nu F_{\text{eq}} x^\ddagger Z}{\Delta G^\ddagger} \right)^{\frac{1}{\nu}}} \right)$$

$\langle F_{\text{Last}} \rangle$ will be given as previously by Eq. (13) using Eq. (18), Eq. (19) and Eq. (20) for $\langle F_{\text{Rev}} \rangle$,

$\langle F_{\text{FirstRef}} \rangle$ and $\langle F_{\text{RevRef}} \rangle$ respectively.

$$\langle F_{\text{FirstRef}} \rangle \approx \frac{\Delta G_{\text{ref}}^{\ddagger}}{\nu x_{\text{ref}}^{\ddagger} Z_{\text{ref}}} \left(\left(Z_{\text{ref}}^2 + \frac{\nu F_{\text{fin}} x_{\text{ref}}^{\ddagger} Z_{\text{ref}}}{\Delta G_{\text{ref}}^{\ddagger}} \right)^{\frac{1}{\nu}} - \frac{k_{\text{B}} T}{\Delta G_{\text{ref}}^{\ddagger}} e^{\frac{k_{0\text{ref}} k_{\text{B}} T}{x_{\text{ref}}^{\ddagger} F Z_{\text{ref}}}} \frac{\frac{\Delta G_{\text{ref}}^{\ddagger}}{k_{\text{B}} T} \left(1 - \left(Z_{\text{ref}}^2 + \frac{\nu F_{\text{fin}} x_{\text{ref}}^{\ddagger} Z_{\text{ref}}}{\Delta G_{\text{ref}}^{\ddagger}} \right)^{\frac{1}{\nu}} \right)}{E_1 \left(\frac{k_{0\text{ref}} k_{\text{B}} T}{x_{\text{ref}}^{\ddagger} F Z_{\text{ref}}} e^{\frac{\Delta G_{\text{ref}}^{\ddagger}}{k_{\text{B}} T} \left(1 - \left(Z_{\text{ref}}^2 + \frac{\nu F_{\text{fin}} x_{\text{ref}}^{\ddagger} Z_{\text{ref}}}{\Delta G_{\text{ref}}^{\ddagger}} \right)^{\frac{1}{\nu}} \right)} \right)} \right)^{\nu} - Z_{\text{ref}}^2 \right)$$

$$\theta \left(\dot{F}_{\text{cFirst}} - \dot{F} \right) + \left(-\frac{\Delta G_{\text{ref}}^{\ddagger} Z_{\text{ref}}}{\nu x_{\text{ref}}^{\ddagger}} + \sqrt{2 \dot{F}_{\text{cFirst}} x_{\text{ref}}^{\ddagger} \zeta} - \sqrt{2 \dot{F} x_{\text{ref}}^{\ddagger} \zeta} \right) \cdot \theta \left(\dot{F} - \dot{F}_{\text{cFirst}} \right)$$
(19)

Where $\dot{F}_{\text{cFirst}} = \frac{k_{0\text{ref}} k_{\text{B}} T e^{\frac{\Delta G_{\text{ref}}^{\ddagger}}{k_{\text{B}} T} + \gamma}}{x_{\text{ref}}^{\ddagger} Z_{\text{ref}}} \left(1 - e^{-\frac{\Delta G_{\text{ref}}^{\ddagger}}{k_{\text{B}} T} \left(Z_{\text{ref}}^2 + \frac{\nu F_{\text{fin}} x_{\text{ref}}^{\ddagger} Z_{\text{ref}}}{\Delta G_{\text{ref}}^{\ddagger}} \right)^{\frac{1}{\nu}}} \right)$ and $Z_{\text{ref}} = 1 + \frac{\kappa}{\kappa_{G_{0\text{ref}}}(x_{\text{min}})}$ where

$\kappa_{G_{0\text{ref}}}(x_{\text{min}}) \equiv \left. \frac{\partial^2 G_{0\text{ref}}(x)}{\partial x^2} \right|_{x=x_{\text{min}}}$ is the curvature of the free energy profile at the unfolded state and

$G_{0\text{ref}}(x) = \Delta G_{\text{ref}}^{\ddagger} \frac{\nu}{1-\nu} \left(\frac{x}{x_{\text{ref}}^{\ddagger}} \right)^{\frac{1}{1-\nu}} - \frac{\Delta G_{\text{ref}}^{\ddagger}}{\nu} \frac{x}{x_{\text{ref}}^{\ddagger}}$ is the model for the free energy profile. For the linear-

cubic free energy profile Z_{ref} reduce to $Z_{\text{ref}} = 1 - \frac{\kappa x_{\text{ref}}^{\ddagger 2}}{6 \Delta G_{\text{ref}}^{\ddagger}}$.

$$\langle F_{\text{RevRef}} \rangle \approx \frac{\Delta G_{\text{ref}}^{\ddagger}}{\nu x_{\text{ref}}^{\ddagger} Z_{\text{ref}}} \left(\left(Z_{\text{ref}}^2 + \frac{\nu F_{\text{eq}} x_{\text{ref}}^{\ddagger} Z_{\text{ref}}}{\Delta G_{\text{ref}}^{\ddagger}} \right)^{\frac{1}{\nu}} - \frac{k_{\text{B}} T}{\Delta G_{\text{ref}}^{\ddagger}} e^{\frac{k_{0\text{ref}} k_{\text{B}} T}{x_{\text{ref}}^{\ddagger} F Z_{\text{ref}}}} \frac{\frac{\Delta G_{\text{ref}}^{\ddagger}}{k_{\text{B}} T} \left(1 - \left(Z_{\text{ref}}^2 + \frac{\nu F_{\text{eq}} x_{\text{ref}}^{\ddagger} Z_{\text{ref}}}{\Delta G_{\text{ref}}^{\ddagger}} \right)^{\frac{1}{\nu}} \right)}{E_1 \left(\frac{k_{0\text{ref}} k_{\text{B}} T}{x_{\text{ref}}^{\ddagger} F Z_{\text{ref}}} e^{\frac{\Delta G_{\text{ref}}^{\ddagger}}{k_{\text{B}} T} \left(1 - \left(Z_{\text{ref}}^2 + \frac{\nu F_{\text{eq}} x_{\text{ref}}^{\ddagger} Z_{\text{ref}}}{\Delta G_{\text{ref}}^{\ddagger}} \right)^{\frac{1}{\nu}} \right)} \right)} \right)^{\nu} - Z_{\text{ref}}^2 \right)$$

$$\theta \left(\dot{F}_{\text{cRevRef}} - \dot{F} \right) + \left(-\frac{\Delta G_{\text{ref}}^{\ddagger} Z_{\text{ref}}}{\nu x_{\text{ref}}^{\ddagger}} + \sqrt{2 \dot{F}_{\text{cRevRef}} x_{\text{ref}}^{\ddagger} \zeta} - \sqrt{2 \dot{F} x_{\text{ref}}^{\ddagger} \zeta} \right) \cdot \theta \left(\dot{F} - \dot{F}_{\text{cRevRef}} \right)$$
(20)

Where $\dot{F}_{\text{cRevRef}} = \frac{k_{0\text{ref}} k_{\text{B}} T e^{\frac{\Delta G_{\text{ref}}^{\ddagger}}{k_{\text{B}} T} + \gamma}}{x_{\text{ref}}^{\ddagger} Z_{\text{ref}}} \left(1 - e^{-\frac{\Delta G_{\text{ref}}^{\ddagger}}{k_{\text{B}} T} \left(Z_{\text{ref}}^2 + \frac{\nu F_{\text{eq}} x_{\text{ref}}^{\ddagger} Z_{\text{ref}}}{\Delta G_{\text{ref}}^{\ddagger}} \right)^{\frac{1}{\nu}}} \right)$. As previously F_{eq} in the case of the

mean last unfolding force is not an independent parameter and can be expressed through other parameters of the system (34)

$$F_{\text{eq}} = \int_0^{\infty} \frac{1}{1 + e^{\frac{F^2 - (\Delta G^\ddagger - \Delta G_{\text{ref}}^\ddagger)}{2\kappa k_{\text{B}} T}}} = -\sqrt{\frac{\pi\kappa k_{\text{B}} T}{2}} \text{Li}_{1/2} \left(-e^{\frac{\Delta G^\ddagger - \Delta G_{\text{ref}}^\ddagger}{k_{\text{B}} T}} \right) \text{ where } \text{Li}_{1/2}(\cdot) \text{ is the polylogarithm (11).}$$

In order to see how well different models predict mean unfolding force dependence on the loading rate when the pulling force is applied through spring, we carried out BD simulations where we pulled with constant speed on Morse free energy profile through spring. The spring constant was 100 pN/nm and Morse free energy profile parameters were chosen as in (33). We generated 3000 trajectories for each loading rate, for the loading rates ranging 11 orders of magnitude Fig. 5 (see methods section for details).

For showing how well do models predict mean unfolding force dependence on the loading rate we plot models predictions and the data from the BD simulations on the same graph Fig. 5. The parameters for plotting the models were the same as in the BD simulations. Further to quantify how well do models predict BD simulations data we have calculated R^2 and χ^2 (see methods section for details) in Table 2. Unified models (2019) are generally giving the best predictions. As it appears the soft spring approximation works well in this case since Z is close to 1 and we could have used models that do not take into account the correction for spring. However since the reversible model (33, 34) was developed originally assuming pulling through spring, we used models that take into account the effect of spring in order to have all models in the equal ground.

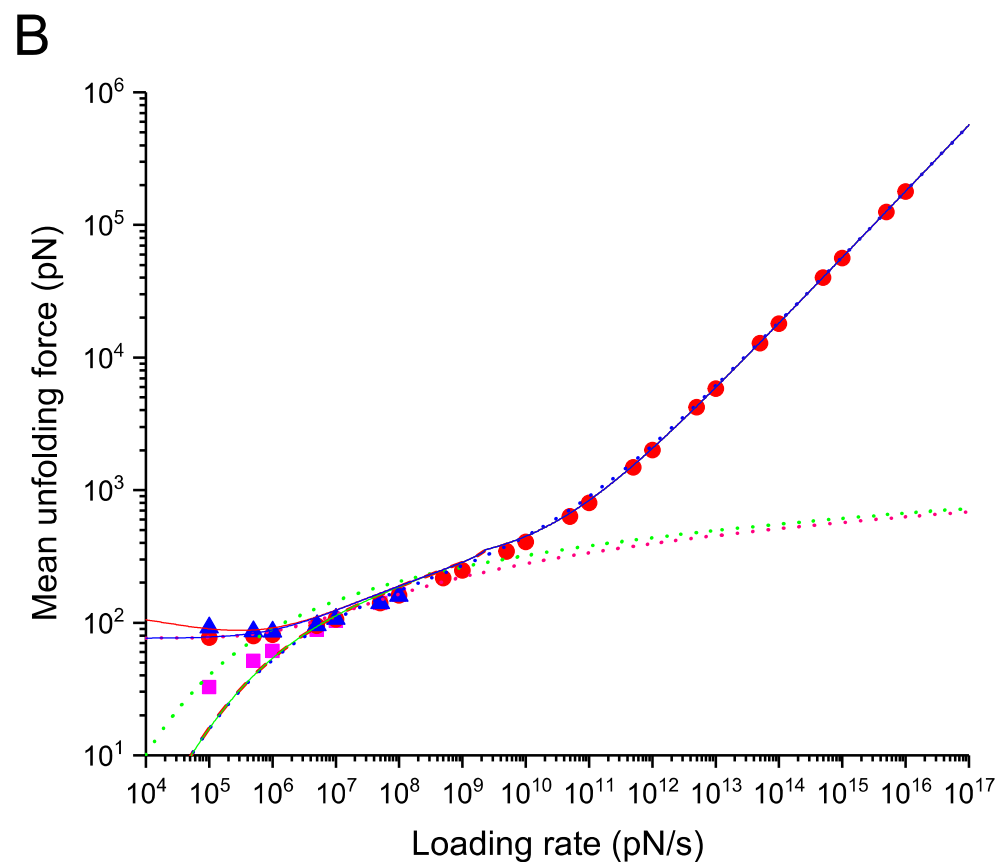
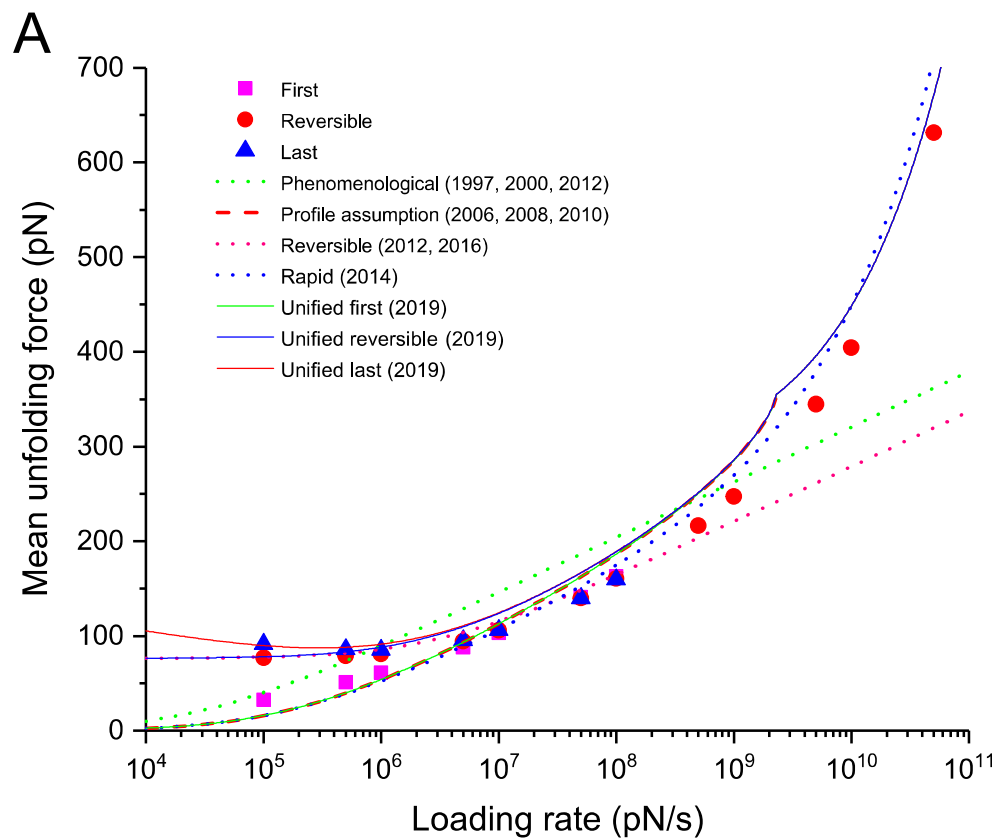


Figure 5. Mean unfolding force dependence on the loading rate from BD simulations with Morse free energy profile and the predictions from the DFS models. (B) shows the log-log plot for the data as in (A) but for the larger range of the loading rates. Three regimes can be distinguished from (B). Low loading rate regime is where three differently defined mean unfolding forces diverge this regime ends roughly where the mean last unfolding force has a minimum, the mean reversible unfolding force rises from the constant F_{eq} value and the mean first unfolding force follows different slope, around $5 \cdot 10^6$ pN/s. The intermediate loading rate regime starts where the low loading rate regime ends and ends roughly where the change in the slope can be noticed around 10^{10} pN/s, indicating that unfolding occurs after the barrier is disappeared. The models are plotted using the parameters from the BD simulation (hence these are NOT fits). Phenomenological (1997, 2000, 2012) represents Eq. (7), profile assumption (2006, 2008, 2010) represents Eq. (8), reversible (2012, 2016) represents Eq. (6), rapid (2014) represents Eq. (10), unified first (2019) represents Eq. (17), unified reversible (2019) represents Eq. (18), unified last (2019) represents Eq. (13) where Eq. (18), Eq. (19) and Eq. (20) were used. Table 2 shows how well models predict the data from this figure. The parameters used in models were $k_B T = 4.1$ pN nm, $\kappa = 100$ pN/nm, $x^\ddagger = 0.162$ nm, $k_0 = 5002.51$ s⁻¹, $\Delta G^\ddagger = 37.85$ pN nm, $\zeta = 10^5$ pN s/nm, $F_{eq} = 76.4$ pN, $F_{fin} = 150$ pN, $\nu = 0.66667$, $x_{ref}^\ddagger = 0.338$ nm, $k_{0ref} = 550713$ s⁻¹, $\Delta G_{ref}^\ddagger = 8.4$ pN nm. The error bars for the standard error of the mean are smaller than the symbols.

Model	Low loading rates ($\dot{F} < 10^7$ pN/s)		Intermediate loading rates (10^7 pN/s $\leq \dot{F}$ $\leq 10^{10}$ pN/s)		High loading rates ($\dot{F} > 10^{10}$ pN/s)		All loading rates	
	R ²	χ^2	R ²	χ^2	R ²	χ^2	R ²	χ^2
Phenomenological (1997, 2000, 2012)	-0.8937	8.5561	0.7867	8.6606	-0.4415	2534.49	-0.1848	2550.6
Profile assumption (2006, 2010)	0.6993	2.5944	1.0765+ 0.0716i	0.6246- 1.0892	-0.4428- 0.0096i	2513.46+ 112.249i	- 0.1859- 0.0079i	2517.91+ 111.189i
Rapid (2014)	0.6861	2.726	0.9396	1.2329	0.9995	4.8118	0.9996	8.459
Unified first (2019)	0.6993	2.5944	0.8855	3.0696	0.9996	1.2131	0.9997	6.5727
Reversible (2012, 2016)	0.3416	1.2726	0.6724	4.6319	-0.4426	2554.35	-0.1858	2560.25
Unified reversible (2019)	-0.6159	2.7631	0.8735	4.1891	0.9996	1.2143	0.9997	8.1665
Unified last (2019)	-3.0559	1.5944	0.8723	4.275	0.9996	1.2144	0.9997	7.8419

Table 2. For quantifying how well models predict the simulated data we calculated R^2 and χ^2 (see Methods section) for each model plotted in Fig. 5 at three regimes first separately and then all together (last column). Profile assumption (2006, 2010) model predicts complex values for the mean unfolding force at high loading rates, we present R^2 and χ^2 for this model too for completeness. Perfect prediction would result in $R^2 = 1$ and $\chi^2 = 0$.

Distributions of differently defined unfolding forces

The distributions of differently defined unfolding forces at low loading rate regime are vastly different Fig. 6. Reversible unfolding force is symmetric and narrowly distributed around its mean. Last unfolding force is more widely distributed and has a right tail. Generally at the intermediate loading rates, in case of single transition, unfolding force distribution has a left tail (14–18). When there is hopping the first unfolding force also shows a left tail, however as the loading rate decreases the distribution, as a whole, moves closer to 0 and the left tail disappears, this can be seen in Fig. 6A. The evolution of the differently defined unfolding force distributions over the loading rate is an interesting question since distributions are very different at the close to equilibrium regime and eventually they coincide as the system moves further from equilibrium. A subject of the future research could be the derivation of a differential equation describing this “dynamics”.

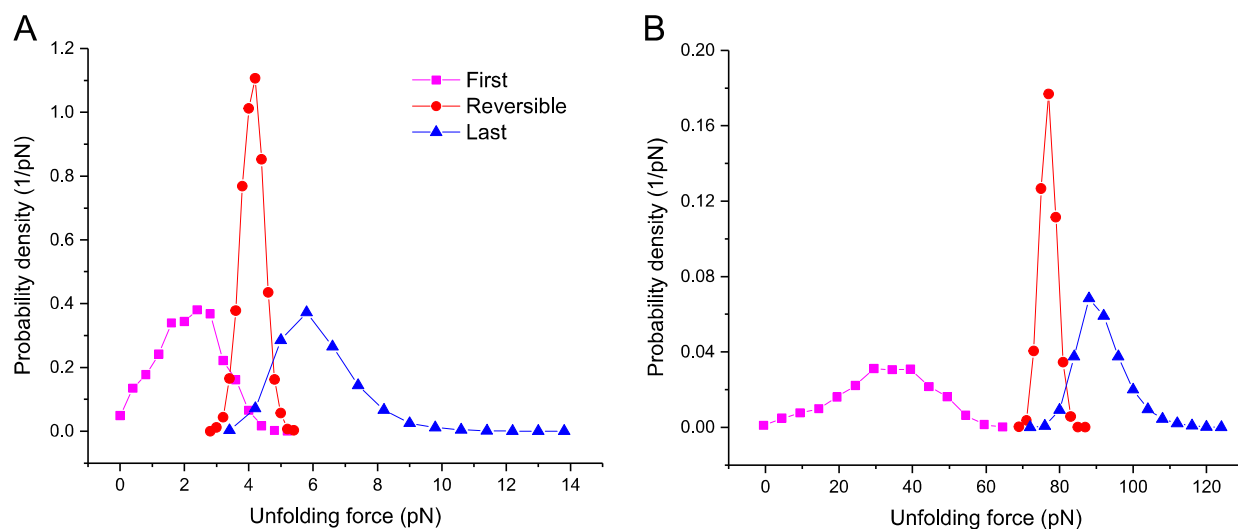


Figure 6. Distributions of first, reversible and last unfolding forces obtained from BD simulations on quartic free energy profile with 100 pN/s loading rate (A) and on Morse free energy profile where force is applied through spring with stiffness of 100 pN/nm that was pulled with speed of 1000 nm/s (B). Last unfolding force shows a left tail, reversible unfolding force is symmetric around its mean and is most compact. Characteristic left tail of the first unfolding force distribution disappears at such low loading rates.

Mean last unfolding force behavior at low loading rates

As we have already mentioned the mean last unfolding force starts to increase with the decrease of the loading rate at the low loading rate regime. Performing BD simulations at lower loading rates is challenging due to the required long simulation time and large memory. However, we could see the prediction of the unified model for the mean last unfolding force at lower loading rates Fig. 7.

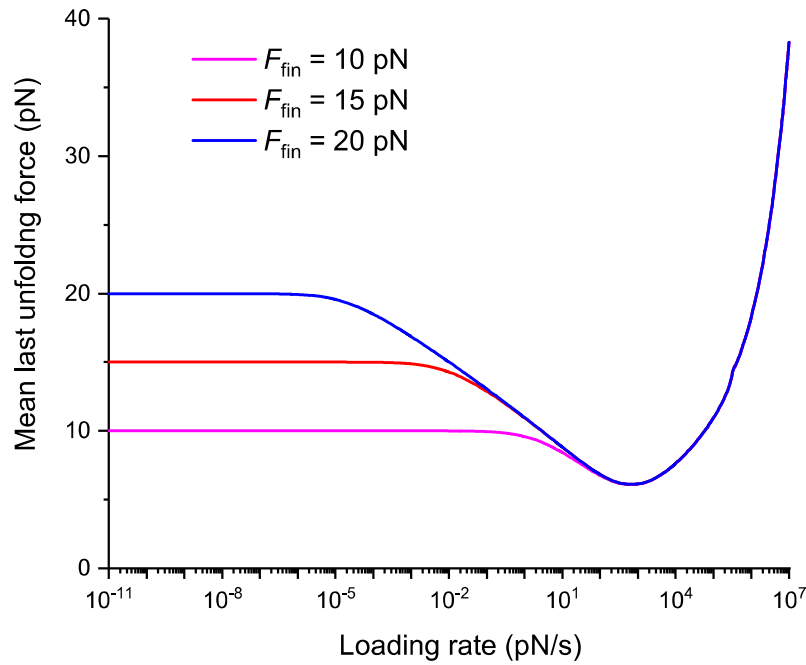


Figure 7. Mean last unfolding force dependence on the loading rate for very low loading rates from the unified model. For very low loading rates mean last unfolding force tends to the constant value of final force (F_{fin}) that is force till which the system is driven. Final force is not an intrinsic parameter of the system but is set by the experimenter and can be higher than the critical force (force at which barrier disappears). Figure generated using Eq. (13) with Eq. (12), Eq. (14) and Eq. (15) in it, with parameter values $k_B T = 4.1$ pN nm, $x^\ddagger = 4.27$ nm, $k_0 = 9.33$ s⁻¹, $\Delta G^\ddagger = 40.62$ pN nm, $\zeta = 10^{-5}$ pN s/nm, $F_{eq} = 4.02$ pN, $\nu = 0.66667$, $x_{ref}^\ddagger = 2.74$ nm, $k_{0ref} = 6495$ s⁻¹, $\Delta G_{ref}^\ddagger = 12.41$ pN nm.

We first observe increase and then a plateau of the mean last unfolding force at low loading rates. This means that the time for the last unfolding increases with the decrease in the

loading rate so that the product of that time and the loading rate still increases. When the loading rate tends to 0 $\langle F_{\text{FirstRef}} \rangle$ Eq. (14) tends to F_{fin} i.e. the final force till which the pulling continuous or the force from where the refolding could stats. At the same limit $\langle F_{\text{Rev}} \rangle$ Eq. (12) and $\langle F_{\text{RevRef}} \rangle$ Eq. (15) both tend to the same constant F_{eq} hence $\langle F_{\text{Last}} \rangle$ Eq. (13) will tend to F_{fin} as $\langle F_{\text{FirstRef}} \rangle$. The plateau is an indication that after some value of the loading rate, for the lower loading rates, the hopping continuous until the end of the process, i.e. until the final force to which the system is driven. This is happening since there is always a finite probability for the system to refold back and unfold again even if the energy of the native state became much higher than that of unfolded state during the pulling process. It is a matter of time for such improbable events to occur during the entire pulling process, and at low enough loading rates there is enough time for that.

Discussion

It is crucial to understand that different models might be using different definitions of the unfolding forces. As it was shown in Fig. 3 and Fig. 5 differently defined mean unfolding forces are very different at low loading rate regime. Nevertheless the reversible model (33, 34) has been widely used for fitting the mean unfolding force dependence on the loading rate without specifying how the unfolding forces were determined (13, 38–40). It is possible that data was collected from the medium and high loading rate regimes where hopping is not observed, however, if there is a lack of data from all three regimes some of the parameters cannot be estimated reliably. For example, if there is no data from the low loading rate regime (where the hopping occurs) then the parameters describing the equilibrium properties of the system (such as F_{eq} , $x^{\ddagger} + x_{\text{ref}}^{\ddagger}$ and $\Delta G^{\ddagger} - \Delta G_{\text{ref}}^{\ddagger}$) could not be reliably estimated. The detection of the hopping is not only related to the lower loading rates but also requires a higher signal to noise ratio and temporal resolution. For example in mechanical unfolding studies of bacteriorhodopsin through AFM from the freely spanning membrane which lowers the loading rates considerably, we did not observe hopping (41). However, using modified cantilevers which significantly increase the temporal resolution hopping and new intermediates in bacteriorhodopsin unfolding have been observed at higher loading rates (29, 42). Hereby we encourage researchers (28, 29, 42) that

possess the data or capability of acquiring data where they detect hopping for a large enough range of the loading rates to test the predictions of the unified model for the mean last unfolding force.

The little cusp in the unified models at the transition from intermediate to the high loading rates (see Fig. 3A and Fig. 5A) is a consequence of using the profile assumption model (15, 22) which in its turn uses the Kramers high barrier approximation (20). The barrier gets lower under the externally applied force and that approximation breaks down before but close to the critical force. In the current study, the unification of the mean unfolding force dependence on the loading rate for the low and intermediate loading rate regimes with the high loading rate regime was done using a mathematical trick. In order to have a full physical description, we need an analytical and analytically integrable expression for the unfolding rate dependence on the force that will avoid the Kramers high barrier approximation and will be valid for the whole range of the forces even above the critical force.

Methods

Brownian dynamics simulations

Two sets of BD simulations were carried out. In the first set, the quartic free energy profile was ramped with the constant loading rate ranging from 10 pN/s to 10^{12} pN/s to the final force of 15 pN for the low loading rates Eq. (21). In the second set of simulations, Morse free energy profile was pulled through spring, with spring constant of 100 pN/nm, with the constant velocity ranging from 1000 nm/s to 10^{14} nm/s to the final force of 150 pN for the low loading rates Eq. (22). The friction coefficient was chosen to be 10^{-5} pN s/nm (43) in both sets of simulations the overdamped Langevin equation Eq. (23) was solved numerically using Euler–Maruyama method.

$$G(x, t) = 100 \left(\left(\frac{x}{5} \right)^4 - \left(\frac{x}{5} \right)^2 \right) + 4x - \dot{F} t x \quad (21)$$

$$G(x,t) = 41 \left(1 - e^{-2 \left(\frac{x-1}{0.1} \right)^2} \right) - 41 + \frac{\kappa}{2} (Vt - x + 0.1)^2 \quad (22)$$

Where t is the time and V is the speed with which spring is pulled.

$$\zeta \dot{x}(t) = -\frac{\partial G(x,t)}{\partial x} + \sqrt{2\zeta k_B T} R(t) \quad (23)$$

Where $R(t)$ is a delta-correlated Gaussian white noise with 0 mean. The simulation time step for the quartic free energy profile was chosen to be 10^{-9} s and for the Morse free energy profile was chosen to be 10^{-12} s, securing less than 10 % of error due to finite time step (44). For high loading rates where the simulation time becomes quite short, the time steps were decreased even more, securing that at least half a million steps were in a trajectory (random walk as a limit of Brownian motion, Donker's theorem). For each loading rate, 3000 trajectories were generated. For each trajectory, the initial value for the reaction coordinate was chosen randomly from the Boltzmann distribution for the corresponding free energy profiles native state neighborhood. The first, reversible and last unfolding forces have been recorded for each trajectory and the mean unfolding forces were calculated from that data.

Determination of the parameters

To compare how well do models predict the outcome of BD simulations we needed to use the same parameters in the models that were used in the BD simulation. For the BD simulations with the quartic free energy profile most of the parameters could be determined straightforwardly, the determination of others is described here. The energy profile parameter (μ) for the profile assumption (2016) model (23) was determined by fitting the free energy profile model proposed in (23) to the part of the quartic free energy profile. The unfolding rate has been determined using Eq. (24), Fig. 8 (21, 45–47), the refolding rate have been calculated using a similar equation.

$$k = \frac{k_B T}{\zeta} \cdot \frac{1}{\int_{x_{\min}}^b e^{\frac{G(y)}{k_B T}} dy \int_a^y e^{\frac{G(z)}{k_B T}} dz dy} \quad (24)$$

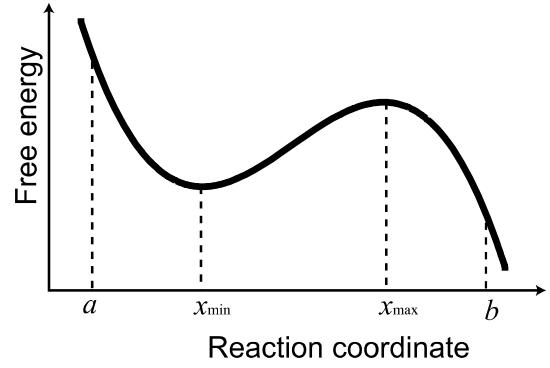


Figure 8. The unfolding rate can be calculated using Eq. (24) where the integration limits are shown in this figure. The refolding rate can be calculated analogously.

Where $G()$ is the free energy profile and a and b are correspondingly reflecting and absorbing boundaries. The equilibrium force was determined assuming the force dependence of the free energy profile in Eq. (24) and numerically solving the equation of the unfolding and refolding rates in order to find the force at which they are equal.

In the case of the Morse free energy profile, the determination of the parameters is less trivial since this profile does not have any barrier in the absence of the external force. In order to find the distance between the native and the transition states for this model, we choose as a barrier position 0.262 nm which is the mean of the barrier positions when it first appears at 0.135 nm and when it disappears at 0.389 nm. Since the native state was at 0.1 nm then $x^\ddagger \approx 0.162$ nm. The unfolded state distance was chosen at 0.6 nm where the second minimum becomes noticeable. Hence for this case as a first unfolding force was taken the product of the time at which system visited the unfolded state (0.6 nm) for the first time and the loading rate, as a last unfolding force was taken the product of the time at which the system was in the native state (0.1 nm) for the last time and the loading rate, and as a reversible unfolding force was taken the product of the loading rate and the time that system spent on the native side of the transition state (time spent for $x < 0.262$ nm). For determining x_{ref}^\ddagger and $\Delta G_{\text{ref}}^\ddagger$ we followed the approach described in (48). For determining the unfolding and refolding rates we used Eq. (24), Fig 8 and the equilibrium force was determined with the same method as in the case of the quartic free energy profile. The determination of the parameter values for the Morse free energy profile is challenging since some parameters are virtual. Our choice of the Morse free energy profile with

spring for this study is due to the historical reasons (33). We could have chosen a different path for determining the parameters of the Morse free energy profile particularly by evaluating first and third derivatives at the inflection point as described in (15), however, parameters determined with this approach might put profile assumption model and related models in a favorable position. To calculate the loading rate ideally $\kappa V/Z$ should be used (4, 35) however we have used κV since in our case $Z \approx 1.00305$ which shows that in this case, the soft spring approximation is applicable.

R² and χ^2 criteria

As goodness of prediction criterion, we used R² defined by Eq. (25).

$$R^2 \equiv 1 - \frac{\sum_{i=1}^n (O_i - E_i)^2}{\sum_{i=1}^n (O_i - \langle O \rangle)^2} \quad (25)$$

Where O_i is the observed value of the i^{th} data point, i.e. the value we get from the data, E_i is the expected value for the i^{th} data point, i.e. the value predicted by the model and $\langle O \rangle$ is the mean of the data (see Fig. 9A). Clearly closer the R² to 1 better the model predicts the data. Model with more parameters is having an advantage when models are being fitted, in such a case adjusted R² might be used which is defined by Eq. (26).

$$\bar{R}^2 \equiv 1 - (1 - R^2) \frac{n-1}{n-p-1} \quad (26)$$

Where R^2 is defined by Eq. (25), n is the sample size (number of data points) and p is the number of parameters in the model.

Another goodness of prediction criterion used in this study is χ^2 defined by Eq. (27).

$$\chi^2 \equiv \sum_{i=1}^n \frac{(O_i - E_i)^2}{\sigma_i^2} \quad (27)$$

Where σ_i is the standard deviation (instead of the standard deviation the standard error or other types of errors are also used for defining χ^2 , however since all our data points are obtained from the averaging of the same number of unfolding forces we use standard deviation) for each data point and the summation goes through the all data points from first to the last (n^{th}) (see Fig. 9B). Clearly close the χ^2 to 0 better the model predicts the data. Similar to adjusted R^2 there is also reduced χ^2 defined by Eq. (28), that takes into account the degrees of freedom of the model.

$$\bar{\chi}^2 \equiv \frac{\chi^2}{n - p - 1} \quad (28)$$

Where χ^2 is given by Eq. (27). In our analyses we have not used adjusted R^2 and reduced χ^2 since we did not fit models to the data i.e. we did not change the parameters of the models to optimize R^2 or χ^2 . From the values in Table 1 and Table 2 and by determining the number of the data points for each range from Fig. 3 and Fig. 5 adjusted R^2 and reduced χ^2 can easily calculate for all models discussed in this work using Eq. (26) and Eq. (28).

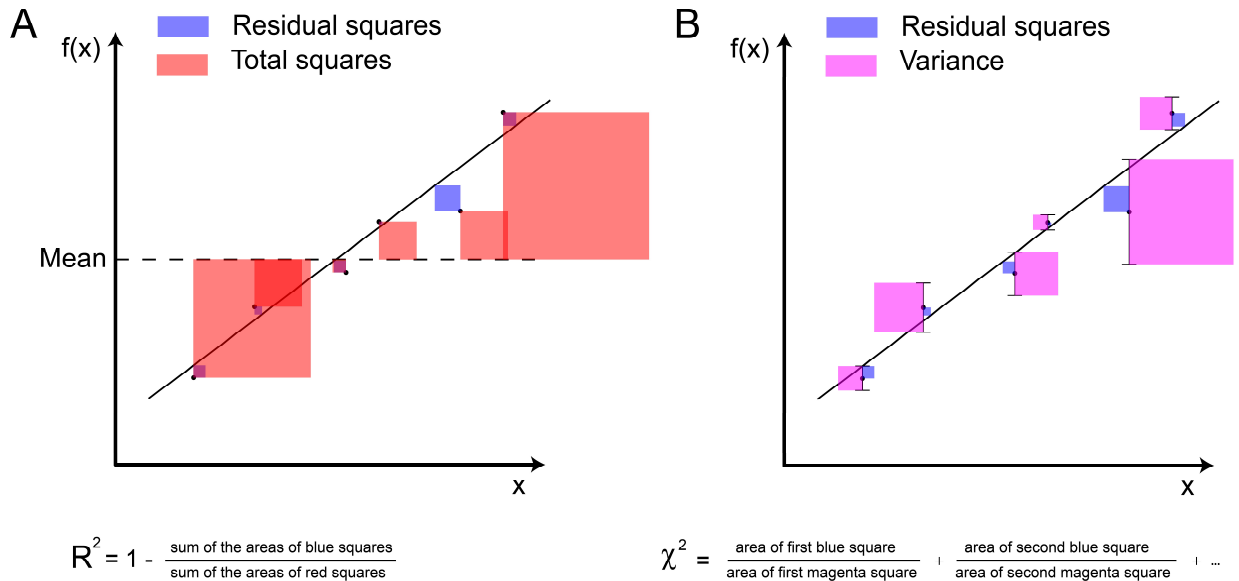


Figure 9. Visualization of the goodness of prediction criterions R^2 Eq. (25) (A) and χ^2 Eq. (27) (B) used in this study. Error bars in (B) show the standard deviations. Closer the R^2 to 1 better the prediction. Closer the χ^2 to 0 better the prediction.

Appendix A

Mean reversible unfolding force dependence on the loading rate for the unified model

The derivation of the Eq. (12) will be shown in two steps. First the calculation of the mean force dependence on the loading rate for the low and intermediate loading rates. Second, we will unite that result with the result of the high loading rates.

For the first part, we follow the approach of (33) with a difference that we use the profile assumption rate expression (15) Eq. (A1) which is more general than the phenomenological rate (6–8) used in (33) and reduces to it when $\nu = 1$.

$$k(F) = k_0 \left(1 - \frac{\nu F x^\ddagger}{\Delta G^\ddagger}\right)^{\frac{1}{\nu}-1} e^{-\frac{\Delta G^\ddagger}{k_B T} \left(1 - \left(1 - \frac{\nu F x^\ddagger}{\Delta G^\ddagger}\right)^{\frac{1}{\nu}}\right)} \quad (\text{A1})$$

$$\int k(F) dF = \frac{k_0 k_B T}{x^\ddagger} e^{-\frac{\Delta G^\ddagger}{k_B T} \left(1 - \left(1 - \frac{\nu F x^\ddagger}{\Delta G^\ddagger}\right)^{\frac{1}{\nu}}\right)} \quad (\text{A2})$$

Using the approach of (33) Eq. (A3) and Eq. (A2) in it we get Eq. (A4).

$$\int_1^p \frac{dp'}{p'} = -\frac{1}{F} \int_{F_{\text{eq}}}^F k(F') dF' \quad (\text{A3})$$

$$\ln p = -\frac{k_0 k_B T}{x^\ddagger \dot{F}} \left(e^{-\frac{\Delta G^\ddagger}{k_B T} \left(1 - \left(1 - \frac{\nu F x^\ddagger}{\Delta G^\ddagger}\right)^{\frac{1}{\nu}}\right)} - e^{-\frac{\Delta G^\ddagger}{k_B T} \left(1 - \left(1 - \frac{\nu F_{\text{eq}} x^\ddagger}{\Delta G^\ddagger}\right)^{\frac{1}{\nu}}\right)} \right) \quad (\text{A4})$$

By solving Eq. (A4) for F we find Eq. (A5).

$$F = \frac{\Delta G^\ddagger}{\nu x^\ddagger} \left(1 - \left(1 - \frac{k_B T}{\Delta G^\ddagger} \ln \left(e^{-\frac{\Delta G^\ddagger}{k_B T} \left(1 - \left(1 - \frac{\nu F_{\text{eq}} x^\ddagger}{\Delta G^\ddagger}\right)^{\frac{1}{\nu}}}\right)} - \frac{x^\ddagger \dot{F} \ln p}{k_0 k_B T} \right) \right)^{\nu} \right) \quad (\text{A5})$$

The advantage of using the rate in Eq. (A1) (15) versus the rate used in (23) where the first power is $2-1/\mu$ instead of $1/\nu-1$ is that the indefinite integral in Eq. (A2) will contain exponential integral (10, 11) which complicates the succeeding step of solving Eq. (A4) for F .

At this step, we follow the approximate averaging procedure as in (22).

$$\alpha \equiv \ln \left(e^{\frac{\Delta G^\ddagger}{k_B T} \left(1 - \left(1 - \frac{\nu F_{\text{eq}} x^\ddagger}{\Delta G^\ddagger} \right)^{\frac{1}{\nu}} \right)} - \frac{x^\ddagger \dot{F} \ln p}{k_0 k_B T} \right)$$

$$\langle F \rangle \approx F(\langle \alpha \rangle)$$

$$\int_0^1 \ln \left(A - \frac{\ln p}{B} \right) dp = e^{AB} E_1(AB) + \ln(A) \approx \ln \left(A + \frac{e^{-\gamma}}{B} \right) \quad (\text{A6})$$

From Eq. (A5) and Eq. (A6) we will obtain for the mean reversible unfolding force the Eq. (A7).

$$\langle F \rangle \approx \frac{\Delta G^\ddagger}{\nu x^\ddagger} \left(1 - \left(1 - \frac{k_B T}{\Delta G^\ddagger} \left(e^{\frac{k_0 k_B T}{x^\ddagger \dot{F}} e^{\frac{\Delta G^\ddagger}{k_B T} \left(1 - \left(1 - \frac{\nu F_{\text{eq}} x^\ddagger}{\Delta G^\ddagger} \right)^{\frac{1}{\nu}} \right)}} E_1 \left(\frac{k_0 k_B T}{x^\ddagger \dot{F}} e^{\frac{\Delta G^\ddagger}{k_B T} \left(1 - \left(1 - \frac{\nu F_{\text{eq}} x^\ddagger}{\Delta G^\ddagger} \right)^{\frac{1}{\nu}} \right)} \right) + \frac{\Delta G^\ddagger}{k_B T} \left(1 - \left(1 - \frac{\nu F_{\text{eq}} x^\ddagger}{\Delta G^\ddagger} \right)^{\frac{1}{\nu}} \right) \right) \right) \right)^\nu \quad (\text{A7})$$

Using the approximation from Eq. (A6) in Eq. (A7) we will get Eq. (A8).

$$\langle F \rangle \approx \frac{\Delta G^\ddagger}{\nu x^\ddagger} \left(1 - \left(1 - \frac{k_B T}{\Delta G^\ddagger} \ln \left(e^{\frac{\Delta G^\ddagger}{k_B T} \left(1 - \left(1 - \frac{\nu F_{\text{eq}} x^\ddagger}{\Delta G^\ddagger} \right)^{\frac{1}{\nu}} \right)} + \frac{x^\ddagger \dot{F} e^{-\gamma}}{k_{0\text{un}} k_B T} \right) \right) \right)^\nu \quad (\text{A8})$$

Notice that Eq. (A7) and Eq. (A8) are valid until the disappearance of the barrier. Mathematically this is demonstrated by the negative values taken to the non-integer power. Next, we determine the loading rate higher from which this occurs.

$$1 - \frac{k_B T}{\Delta G^\ddagger} \ln \left(e^{\frac{\Delta G^\ddagger}{k_B T} \left(1 - \left(1 - \frac{\nu F_{\text{eq}} x^\ddagger}{\Delta G^\ddagger} \right)^{\frac{1}{\nu}} \right)} + \frac{x^\ddagger \dot{F} e^{-\gamma}}{k_0 k_B T} \right) = 0$$

$$e^{\frac{\Delta G^\ddagger}{k_B T} \left(1 - \left(1 - \frac{\nu F_{\text{eq}} x^\ddagger}{\Delta G^\ddagger} \right)^{\frac{1}{\nu}} \right)} + \frac{x^\ddagger \dot{F} e^{-\gamma}}{k_0 k_B T} = e^{\frac{\Delta G^\ddagger}{k_B T}}$$

$$\dot{F} = \frac{k_0 k_B T e^\gamma}{x^\ddagger} \left(e^{\frac{\Delta G^\ddagger}{k_B T}} - e^{\frac{\Delta G^\ddagger}{k_B T} \left(1 - \left(1 - \frac{\nu F_{\text{eq}} x^\ddagger}{\Delta G^\ddagger} \right)^{\frac{1}{\nu}} \right)} \right)$$

$$\dot{F} = \frac{k_0 k_B T e^{\frac{\Delta G^\ddagger}{k_B T} + \gamma}}{x^\ddagger} \left(1 - e^{-\frac{\Delta G^\ddagger}{k_B T} \left(1 - \frac{\nu F_{\text{eq}} x^\ddagger}{\Delta G^\ddagger} \right)^{\frac{1}{\nu}}} \right)$$

At the critical loading rate, the mean reversible unfolding force is approximately $\Delta G^\ddagger / \nu x^\ddagger$ according to Eq. (A7) and Eq. (A8). After the barrier disappearance, the mean unfolding force increases as a square root of the loading rate $\sqrt{2 \dot{F} x^\ddagger \zeta}$ (14, 18). In order to combine these two dependences that are valid for the different loading rate regimes, we take the absolute value of the expression that is raised to the non-integer power in Eq. (A7) and use the Heaviside step function.

$$\langle F_{\text{Rev}} \rangle \approx \frac{\Delta G^\ddagger}{\nu x^\ddagger} \left(1 - \left| 1 - \frac{k_B T}{\Delta G^\ddagger} \left(e^{\frac{k_0 k_B T}{x^\ddagger \dot{F}} e^{\frac{\Delta G^\ddagger}{k_B T} \left(1 - \left(1 - \frac{\nu F_{\text{eq}} x^\ddagger}{\Delta G^\ddagger} \right)^{\frac{1}{\nu}} \right)}} E_1 \left(\frac{k_0 k_B T}{x^\ddagger \dot{F}} e^{\frac{\Delta G^\ddagger}{k_B T} \left(1 - \left(1 - \frac{\nu F_{\text{eq}} x^\ddagger}{\Delta G^\ddagger} \right)^{\frac{1}{\nu}} \right)} \right) + \frac{\Delta G^\ddagger}{k_B T} \left(1 - \left(1 - \frac{\nu F_{\text{eq}} x^\ddagger}{\Delta G^\ddagger} \right)^{\frac{1}{\nu}} \right) \right) \right|^\nu \right)$$

$$\theta \left(\dot{F}_{\text{cRev}} - \dot{F} \right) + \left(\frac{\Delta G^\ddagger}{\nu x^\ddagger} - \sqrt{2 \dot{F}_{\text{cRev}} x^\ddagger \zeta} + \sqrt{2 \dot{F} x^\ddagger \zeta} \right) \cdot \theta \left(\dot{F} - \dot{F}_{\text{cRev}} \right)$$
(A9)

Where $\dot{F}_{\text{cRev}} = \frac{k_0 k_B T e^{\frac{\Delta G^\ddagger}{k_B T} + \gamma}}{x^\ddagger} \left(1 - e^{-\frac{\Delta G^\ddagger}{k_B T} \left(1 - \frac{\nu F_{\text{eq}} x^\ddagger}{\Delta G^\ddagger} \right)^{\frac{1}{\nu}}} \right)$ and $k_0 = \frac{3\Delta G^\ddagger}{\pi \zeta x^{\ddagger 2}} e^{-\frac{\Delta G^\ddagger}{k_B T}}$.

Eq. (A9) can be further simplified to Eq. (12) or using the approximation from Eq. (A6) to Eq. (A10).

$$\langle F_{\text{Rev}} \rangle \approx \frac{\Delta G^\ddagger}{\nu x^\ddagger} \left(1 - \left| 1 - \frac{k_B T}{\Delta G^\ddagger} \ln \left[e^{\frac{\Delta G^\ddagger}{k_B T} \left(1 - \left(1 - \frac{\nu F_{\text{eq}} x^\ddagger}{\Delta G^\ddagger} \right)^{\frac{1}{\nu}}} \right)} + \frac{e^{-\gamma} x^\ddagger \dot{F}}{k_{0\text{un}} k_B T} \right] \right|^\nu \right) \cdot \theta \left(\dot{F}_{\text{cRev}} - \dot{F} \right) + \left(\frac{\Delta G^\ddagger}{\nu x^\ddagger} - \sqrt{2 \dot{F}_{\text{cRev}} x^\ddagger \zeta} + \sqrt{2 \dot{F} x^\ddagger \zeta} \right) \cdot \theta \left(\dot{F} - \dot{F}_{\text{cRev}} \right) \quad (\text{A10})$$

Mean first unfolding force dependence on the loading rate for the unified model

Mean first unfolding force dependence on the loading rate Eq. (11) could be obtained by starting the integration in Eq. (A3) from 0 and following the same steps, or by directly setting $F_{\text{eq}} = 0$ in Eq. (A9) and further simplifying.

Mean last unfolding force dependence on the loading rate for the unified model

Mean first refolding force Eq. (14) and the mean reversible refolding force Eq. (15) that are used for calculating the mean last unfolding force in Eq. (13) can be obtained using the same methods as described above, though using Eq. (A11) for the refolding rate (37) and limits of integration for $\langle F_{\text{FirstRef}} \rangle$ from F_{fin} to F in Eq. (A13) and for $\langle F_{\text{RevRef}} \rangle$ from F_{eq} to F in and similar equation.

$$k_{\text{ref}}(F) = k_{0\text{ref}} \left(1 + \frac{\nu F x_{\text{ref}}^\ddagger}{\Delta G_{\text{ref}}^\ddagger} \right)^{\frac{1}{\nu} - 1} e^{\frac{\Delta G_{\text{ref}}^\ddagger}{k_B T} \left(1 - \left(1 + \frac{\nu F x_{\text{ref}}^\ddagger}{\Delta G_{\text{ref}}^\ddagger} \right)^{\frac{1}{\nu}} \right)} \quad (\text{A11})$$

$$\int k_{\text{ref}}(F)dF = -\frac{k_{0\text{ref}}k_{\text{B}}T}{x_{\text{ref}}^{\ddagger}} e^{\frac{\Delta G_{\text{ref}}^{\ddagger}}{k_{\text{B}}T} \left(1 - \left(1 + \frac{\nu F x_{\text{ref}}^{\ddagger}}{\Delta G_{\text{ref}}^{\ddagger}} \right)^{\frac{1}{\nu}} \right)} \quad (\text{A12})$$

Using Eq. (A12) in Eq. (A13) we get Eq. (A14).

$$\int_1^p \frac{dp'}{p'} = \frac{1}{\dot{F}} \int_{F_{\text{fin}}}^F k_{\text{ref}}(F')dF' \quad (\text{A13})$$

$$\ln p = -\frac{k_{0\text{ref}}k_{\text{B}}T}{x_{\text{ref}}^{\ddagger} \dot{F}} \left(e^{\frac{\Delta G_{\text{ref}}^{\ddagger}}{k_{\text{B}}T} \left(1 - \left(1 + \frac{\nu F x_{\text{ref}}^{\ddagger}}{\Delta G_{\text{ref}}^{\ddagger}} \right)^{\frac{1}{\nu}} \right)} - e^{\frac{\Delta G_{\text{ref}}^{\ddagger}}{k_{\text{B}}T} \left(1 - \left(1 + \frac{\nu F_{\text{fin}} x_{\text{ref}}^{\ddagger}}{\Delta G_{\text{ref}}^{\ddagger}} \right)^{\frac{1}{\nu}} \right)} \right) \quad (\text{A14})$$

By solving Eq. (A14) for F we find Eq. (A15).

$$F = \frac{\Delta G_{\text{ref}}^{\ddagger}}{\nu x_{\text{ref}}^{\ddagger}} \left(\left(1 - \frac{k_{\text{B}}T}{\Delta G_{\text{ref}}^{\ddagger}} \ln \left(e^{\frac{\Delta G_{\text{ref}}^{\ddagger}}{k_{\text{B}}T} \left(1 - \left(1 + \frac{\nu F_{\text{fin}} x_{\text{ref}}^{\ddagger}}{\Delta G_{\text{ref}}^{\ddagger}} \right)^{\frac{1}{\nu}} \right)} - \frac{x_{\text{ref}}^{\ddagger} \dot{F} \ln p}{k_{0\text{ref}} k_{\text{B}} T} \right) \right)^{\nu} - 1 \right) \quad (\text{A15})$$

At this step, we follow the approximate averaging procedure as in (22).

$$\alpha \equiv \ln \left(e^{\frac{\Delta G_{\text{ref}}^{\ddagger}}{k_{\text{B}}T} \left(1 - \left(1 + \frac{\nu F_{\text{fin}} x_{\text{ref}}^{\ddagger}}{\Delta G_{\text{ref}}^{\ddagger}} \right)^{\frac{1}{\nu}} \right)} - \frac{x_{\text{ref}}^{\ddagger} \dot{F} \ln p}{k_{0\text{ref}} k_{\text{B}} T} \right)$$

$$\langle F \rangle \approx F(\langle \alpha \rangle)$$

From Eq. (A15) and Eq. (A6) we will obtain for the mean first refolding force the Eq. (A16).

$$\langle F_{\text{FirstRef}} \rangle \approx \frac{\Delta G_{\text{ref}}^{\ddagger}}{\nu x_{\text{ref}}^{\ddagger}} \left(\left(1 - \frac{k_{\text{B}} T}{\Delta G_{\text{ref}}^{\ddagger}} \left(e^{\frac{k_{0\text{ref}} k_{\text{B}} T}{x_{\text{ref}}^{\ddagger} \dot{F}} e^{\frac{\Delta G_{\text{ref}}^{\ddagger}}{k_{\text{B}} T} \left(1 - \left(1 + \frac{\nu F_{\text{fin}} x_{\text{ref}}^{\ddagger}}{\Delta G_{\text{ref}}^{\ddagger}} \right)^{\frac{1}{\nu}} \right)}} \right) E_1 \left(\frac{k_{0\text{ref}} k_{\text{B}} T}{x_{\text{ref}}^{\ddagger} \dot{F}} e^{\frac{\Delta G_{\text{ref}}^{\ddagger}}{k_{\text{B}} T} \left(1 - \left(1 + \frac{\nu F_{\text{fin}} x_{\text{ref}}^{\ddagger}}{\Delta G_{\text{ref}}^{\ddagger}} \right)^{\frac{1}{\nu}} \right)}} \right) + \frac{\Delta G_{\text{ref}}^{\ddagger}}{k_{\text{B}} T} \left(1 - \left(1 + \frac{\nu F_{\text{fin}} x_{\text{ref}}^{\ddagger}}{\Delta G_{\text{ref}}^{\ddagger}} \right)^{\frac{1}{\nu}} \right) \right) \right)^{\nu} - 1 \right) \quad (\text{A16})$$

Using the approximation from Eq. (A6) in Eq. (A16) we will get Eq. (A17).

$$\langle F_{\text{FirstRef}} \rangle \approx \frac{\Delta G_{\text{ref}}^{\ddagger}}{\nu x_{\text{ref}}^{\ddagger}} \left(\left(1 - \frac{k_{\text{B}} T}{\Delta G_{\text{ref}}^{\ddagger}} \ln \left(e^{\frac{\Delta G_{\text{ref}}^{\ddagger}}{k_{\text{B}} T} \left(1 - \left(1 + \frac{\nu F_{\text{fin}} x_{\text{ref}}^{\ddagger}}{\Delta G_{\text{ref}}^{\ddagger}} \right)^{\frac{1}{\nu}} \right)} + \frac{e^{-\gamma} x_{\text{ref}}^{\ddagger} \dot{F}}}{k_{0\text{ref}} k_{\text{B}} T} \right) \right) - 1 \right) \quad (\text{A17})$$

Next, we find the critical loading rate in the same way as previously.

$$1 - \frac{k_{\text{B}} T}{\Delta G_{\text{ref}}^{\ddagger}} \ln \left(e^{\frac{\Delta G_{\text{ref}}^{\ddagger}}{k_{\text{B}} T} \left(1 - \left(1 + \frac{\nu F_{\text{fin}} x_{\text{ref}}^{\ddagger}}{\Delta G_{\text{ref}}^{\ddagger}} \right)^{\frac{1}{\nu}} \right)} + \frac{e^{-\gamma} x_{\text{ref}}^{\ddagger} \dot{F}}{k_{0\text{ref}} k_{\text{B}} T} \right) = 0$$

$$\dot{F} = \frac{k_{0\text{ref}} k_{\text{B}} T e^{\frac{\Delta G_{\text{ref}}^{\ddagger}}{k_{\text{B}} T} + \gamma}}{x_{\text{ref}}^{\ddagger}} \left(1 - e^{-\frac{\Delta G_{\text{ref}}^{\ddagger}}{k_{\text{B}} T} \left(1 + \frac{\nu F_{\text{fin}} x_{\text{ref}}^{\ddagger}}{\Delta G_{\text{ref}}^{\ddagger}} \right)^{\frac{1}{\nu}}} \right)$$

By combining the two dependences that are valid for the different loading rate regimes as previously, using the Heaviside step function we obtain Eq. (A18).

$$\langle F_{\text{FirstRef}} \rangle \approx \frac{\Delta G_{\text{ref}}^{\ddagger}}{\nu x_{\text{ref}}^{\ddagger}} \left(\left(1 - \frac{k_{\text{B}} T}{\Delta G_{\text{ref}}^{\ddagger}} \left(e^{\frac{k_{0\text{ref}} k_{\text{B}} T}{x_{\text{ref}}^{\ddagger} \dot{F}} e^{\frac{\Delta G_{\text{ref}}^{\ddagger}}{k_{\text{B}} T} \left(1 - \left(1 + \frac{\nu F_{\text{fin}} x_{\text{ref}}^{\ddagger}}{\Delta G_{\text{ref}}^{\ddagger}} \right)^{\frac{1}{\nu}} \right)}} \right) E_1 \left(\frac{k_{0\text{ref}} k_{\text{B}} T}{x_{\text{ref}}^{\ddagger} \dot{F}} e^{\frac{\Delta G_{\text{ref}}^{\ddagger}}{k_{\text{B}} T} \left(1 - \left(1 + \frac{\nu F_{\text{fin}} x_{\text{ref}}^{\ddagger}}{\Delta G_{\text{ref}}^{\ddagger}} \right)^{\frac{1}{\nu}} \right)}} \right) + \frac{\Delta G_{\text{ref}}^{\ddagger}}{k_{\text{B}} T} \left(1 - \left(1 + \frac{\nu F_{\text{fin}} x_{\text{ref}}^{\ddagger}}{\Delta G_{\text{ref}}^{\ddagger}} \right)^{\frac{1}{\nu}} \right) \right) \right)^{\nu} - 1 \right) \cdot$$

$$\theta \left(\dot{F}_{\text{cFirstRef}} - \dot{F} \right) + \left(-\frac{\Delta G_{\text{ref}}^{\ddagger}}{\nu x_{\text{ref}}^{\ddagger}} + \sqrt{2 \dot{F}_{\text{cFirstRef}} x_{\text{ref}}^{\ddagger} \zeta} - \sqrt{2 \dot{F} x_{\text{ref}}^{\ddagger} \zeta} \right) \cdot \theta \left(\dot{F} - \dot{F}_{\text{cFirstRef}} \right) \quad (\text{A18})$$

Where $\dot{F}_{\text{cFirstRef}} = \frac{k_{0\text{ref}} k_B T e^{\frac{\Delta G_{\text{ref}}^\ddagger + \gamma}{k_B T}}}{x_{\text{ref}}^\ddagger} \left(1 - e^{-\frac{\Delta G_{\text{ref}}^\ddagger}{k_B T} \left(1 + \frac{v F_{\text{fin}} x_{\text{ref}}^\ddagger}{\Delta G_{\text{ref}}^\ddagger} \right)^{\frac{1}{v}}} \right)$ and $k_{0\text{ref}} = \frac{3 \Delta G_{\text{ref}}^\ddagger}{\pi \zeta x_{\text{ref}}^\ddagger} e^{-\frac{\Delta G_{\text{ref}}^\ddagger}{k_B T}}$.

Eq. (A18) can be further simplified to Eq. (14) or using the approximation from Eq. (A6) to a similar equation to Eq. (A10).

The mean reversible refolding force dependence on the loading rate Eq. (15) can be obtained by starting the integration in Eq. (A13) from F_{eq} and following the same steps, or by directly setting F_{fin} to F_{eq} in Eq. (A18) and further simplifying.

Appendix B

Mean first unfolding force for the heterogeneous model

First, we would like to notice the identity Eq. (B1), which can be verified by taking the derivative of the right-hand side with respect to F and obtaining the integrand expression.

$$\begin{aligned}
 & \int F \frac{k_0}{\dot{F}} e^{\frac{x^\ddagger F}{k_B T}} \left(1 + H \frac{k_0 k_B T}{\dot{F} x^\ddagger} \left(e^{\frac{x^\ddagger F}{k_B T}} - 1 \right) \right)^{\frac{H+1}{H}} dF = \\
 & = \frac{k_B T}{x^\ddagger \left(\frac{x^\ddagger}{k_B T} - \frac{k_0}{\dot{F}} H \right)} \left(1 + \frac{k_0 k_B T H}{x^\ddagger \dot{F}} \left(e^{\frac{x^\ddagger F}{k_B T}} - 1 \right) \right)^{-\frac{1}{H}} \cdot \\
 & \left(\frac{x^\ddagger F}{k_B T} \left(\frac{k_0}{\dot{F}} H - \frac{x^\ddagger}{k_B T} \right) + \left(1 + \frac{e^{\frac{x^\ddagger F}{k_B T}}}{\frac{x^\ddagger \dot{F}}{k_0 k_B T H} - 1} \right) \left(\frac{x^\ddagger F}{k_B T} \left(\frac{x^\ddagger}{k_B T} - \frac{k_0}{\dot{F}} H \right) - \frac{k_0}{\dot{F}} e^{\frac{x^\ddagger F}{k_B T}} {}_p F_q \left(1, 1, 1 + \frac{1}{H}; 2, 2; -\frac{e^{\frac{x^\ddagger F}{k_B T}}}{1 - \frac{x^\ddagger \dot{F}}{k_0 k_B T H}} \right) \right) \right)
 \end{aligned} \tag{B1}$$

Where ${}_pF_q$ is a generalized hypergeometric function (10, 11). Notice that the first unfolding force PDF for the heterogeneous model (36) was part of the integrand in Eq. (B1) and the mean first unfolding force can be directly calculated Eq. (B2).

$$\langle F \rangle = \int_0^\infty F \frac{k_0}{\dot{F}} e^{\frac{x^\ddagger F}{k_B T}} \left(1 + H \frac{k_0 k_B T}{\dot{F} x^\ddagger} \left(e^{\frac{x^\ddagger F}{k_B T}} - 1 \right) \right)^{\frac{H+1}{H}} dF = \frac{k_B T H}{x^\ddagger} \left(\frac{k_0 k_B T H}{\dot{F} x^\ddagger} \right)^{-\frac{1}{H}} {}_2F_1 \left(\frac{1}{H}, \frac{1}{H}; 1 + \frac{1}{H}; 1 - \frac{\dot{F} x^\ddagger}{k_0 k_B T H} \right) \quad (\text{B2})$$

An approximate mean reversible unfolding force can also be derived for this model following the approach described in Appendix A. First we notice that the effective rate Eq. (B4) for the heterogeneous model can be written using the profile assumption rate Eq. (A1) (15) in Eq. (B3). The definition of $\Omega(F)$ is given in (36).

$$\Omega(F) \approx \frac{\dot{F}}{H} \ln \left(1 + \frac{H \int_0^F k(F') dF'}{x^\ddagger \dot{F}} \right) \quad (\text{B3})$$

$$k_{\text{eff}}(F) = \frac{d\Omega(F)}{dF} \quad (\text{B4})$$

$$\int k_{\text{eff}}(F) dF = \Omega(F) \approx \frac{\dot{F}}{H} \ln \left(1 + \frac{k_0 k_B T H e^{\frac{\Delta G^\ddagger}{k_B T} \left(1 - \left(1 - \frac{\nu F x^\ddagger}{\Delta G^\ddagger} \right)^{\frac{1}{\nu}} \right)}}{x^\ddagger \dot{F}} \right) \quad (\text{B5})$$

Using the approach of (33) Eq. (A3) and Eq. (B5) in it, we get Eq (B6).

$$\ln p = -\frac{1}{H} \left(\ln \left(1 + \frac{k_0 k_B T H e^{\frac{\Delta G^\ddagger}{k_B T} \left(1 - \left(1 - \frac{\nu F x^\ddagger}{\Delta G^\ddagger} \right)^{\frac{1}{\nu}} \right)}}{x^\ddagger \dot{F}} \right) - \ln \left(1 + \frac{k_0 k_B T H e^{\frac{\Delta G^\ddagger}{k_B T} \left(1 - \left(1 - \frac{\nu F_{\text{eq}} x^\ddagger}{\Delta G^\ddagger} \right)^{\frac{1}{\nu}} \right)}}{x^\ddagger \dot{F}} \right) \right) \quad (\text{B6})$$

By solving Eq. (B6) for F we find Eq. (B7).

$$F = \frac{\Delta G^\ddagger}{\nu x^\ddagger} - \frac{\Delta G^\ddagger}{\nu x^\ddagger} \left(1 - \frac{k_B T}{\Delta G^\ddagger} \ln \left(\frac{x^\ddagger \dot{F}}{k_0 k_B T H} \left(p^{-H} \left(1 + \frac{k_0 k_B T H e^{\frac{\Delta G^\ddagger}{k_B T} \left(1 - \left(1 - \frac{\nu F_{\text{eq}} x^\ddagger}{\Delta G^\ddagger} \right)^{\frac{1}{\nu}}} \right)} \right) - 1 \right) \right) \right)^\nu \quad (\text{B7})$$

At this step, we follow the approximate averaging procedure as in (22).

$$\alpha \equiv \ln \left(\frac{x^\ddagger \dot{F}}{k_0 k_B T H} \left(p^{-H} \left(1 + \frac{k_0 k_B T H e^{\frac{\Delta G^\ddagger}{k_B T} \left(1 - \left(1 - \frac{\nu F_{\text{eq}} x^\ddagger}{\Delta G^\ddagger} \right)^{\frac{1}{\nu}}} \right)} \right) - 1 \right) \right)$$

$$\langle F \rangle \approx F(\langle \alpha \rangle)$$

$$\int_0^1 \ln \left(A \left(1 + \frac{1}{B} \right) p^{-H} - 1 \right) dp = H + \left(-\frac{1}{B} - 1 \right)^{\frac{1}{H}} \pi \csc \left(\frac{\pi}{H} \right) - H_2 F_1 \left(1, -\frac{1}{H}; \frac{H-1}{H}; 1 + \frac{1}{B} \right) + \ln \left(\frac{A}{B} \right) \quad (\text{B8})$$

From Eq. (B7) and Eq. (B8) we will obtain for the mean reversible unfolding force Eq. (B9).

$$\langle F_{\text{Rev}} \rangle \approx \frac{\Delta G^\ddagger}{\nu x^\ddagger} \cdot \left(1 - \left(1 - \frac{k_B T}{\Delta G^\ddagger} \left(H + \left(-\frac{1}{B} - 1 \right)^{\frac{1}{H}} \pi \csc \left(\frac{\pi}{H} \right) - H_2 F_1 \left(1, -\frac{1}{H}; \frac{H-1}{H}; 1 + \frac{k_0 k_B T H e^{\frac{\Delta G^\ddagger}{k_B T} \left(1 - \left(1 - \frac{\nu F_{\text{eq}} x^\ddagger}{\Delta G^\ddagger} \right)^{\frac{1}{\nu}}} \right)} \right) \right) \right)^\nu + \frac{\Delta G^\ddagger}{k_B T} \left(1 - \left(1 - \frac{\nu F_{\text{eq}} x^\ddagger}{\Delta G^\ddagger} \right)^{\frac{1}{\nu}} \right) \quad (\text{B9})$$

The next step as in Appendix A would be the determination of the critical loading rate, in order to extend the model for the high loading rate regime. In this case, we need to solve a transcendental equation involving hypergeometric function. It might be possible to find appropriate approximation and solve that equation for the loading rate, however, this is not in the scope of the current study. Moreover, our simulations do not involve any heterogeneity i.e. the system was in the same native state prior to the pulling process. Once the critical loading rate is determined and the mean reversible unfolding force dependence on the loading rate is extended also for high loading rates, the first unfolding force can be found simply by setting $F_{\text{eq}} = 0$ as in Appendix A. The mean last unfolding force can be found again through Eq. (13) where $\langle F_{\text{FirstRef}} \rangle$ and $\langle F_{\text{RevRef}} \rangle$ can be calculated using the refolding rate expression Eq. (A11) and the same approach as described in the current appendix and Appendix A.

Appendix C

Mean reversible unfolding force dependence on the loading rate for the unified model when the force is applied through spring

When the force is being applied through spring we need to use an appropriate expression for the force-dependent unfolding rate Eq. (C1) (35), which then can be plugged into Eq. (C2).

$$k(F) = k_0 \left(Z^2 - \frac{\nu F x^\ddagger Z}{\Delta G^\ddagger} \right)^{\frac{1}{\nu} - 1} e^{\frac{\Delta G^\ddagger}{k_B T} \left(1 - \left(Z^2 - \frac{\nu F x^\ddagger Z}{\Delta G^\ddagger} \right)^{\frac{1}{\nu}} \right)} \quad (\text{C1})$$

$$\int k(F) dF = \frac{k_0 k_B T}{x^\ddagger Z} e^{\frac{\Delta G^\ddagger}{k_B T} \left(1 - \left(Z^2 - \frac{\nu F x^\ddagger Z}{\Delta G^\ddagger} \right)^{\frac{1}{\nu}} \right)} \quad (\text{C2})$$

Using the approach of (33) Eq. (C3) and Eq. (C2) in it we get Eq. (C4).

$$\int_1^p \frac{dp'}{p'} = -\frac{1}{\dot{F}} \int_{F_{\text{eq}}}^F k(F') dF' \quad (\text{C3})$$

$$\ln p = -\frac{k_0 k_B T}{x^\ddagger Z F} \left(e^{\frac{\Delta G^\ddagger}{k_B T} \left(1 - \left(Z^2 - \frac{\nu F x^\ddagger Z}{\Delta G^\ddagger} \right)^{\frac{1}{\nu}} \right)} - e^{\frac{\Delta G^\ddagger}{k_B T} \left(1 - \left(Z^2 - \frac{\nu F_{\text{eq}} x^\ddagger Z}{\Delta G^\ddagger} \right)^{\frac{1}{\nu}} \right)} \right) \quad (\text{C4})$$

By solving Eq. (C4) for F we find Eq. (C5).

$$F = \frac{\Delta G^\ddagger}{\nu x^\ddagger Z} \left(Z^2 - \left(1 - \frac{k_B T}{\Delta G^\ddagger} \ln \left(e^{\frac{\Delta G^\ddagger}{k_B T} \left(1 - \left(Z^2 - \frac{\nu F x^\ddagger Z}{\Delta G^\ddagger} \right)^{\frac{1}{\nu}} \right)} - \frac{x^\ddagger F Z \ln p}{k_0 k_B T} \right) \right) \right)^\nu \quad (\text{C5})$$

At this step, we follow the approximate averaging procedure as in (22).

$$\alpha \equiv \ln \left(e^{\frac{\Delta G^\ddagger}{k_B T} \left(1 - \left(Z^2 - \frac{\nu F_{\text{eq}} x^\ddagger Z}{\Delta G^\ddagger} \right)^{\frac{1}{\nu}} \right)} - \frac{x^\ddagger F Z \ln p}{k_0 k_B T} \right)$$

$$\langle F \rangle \approx F(\langle \alpha \rangle)$$

From Eq. (C5) and Eq. (A6) we will obtain for the mean reversible unfolding force Eq. (C6).

$$\langle F \rangle \approx \frac{\Delta G^\ddagger}{\nu x^\ddagger Z} \left(Z^2 - \left(1 - \frac{k_B T}{\Delta G^\ddagger} \left(e^{\frac{k_0 k_B T}{x^\ddagger F Z} e^{\frac{\Delta G^\ddagger}{k_B T} \left(1 - \left(Z^2 - \frac{\nu F_{\text{eq}} x^\ddagger Z}{\Delta G^\ddagger} \right)^{\frac{1}{\nu}} \right)}} E_1 \left(\frac{k_0 k_B T}{x^\ddagger F Z} e^{\frac{\Delta G^\ddagger}{k_B T} \left(1 - \left(Z^2 - \frac{\nu F_{\text{eq}} x^\ddagger Z}{\Delta G^\ddagger} \right)^{\frac{1}{\nu}} \right)} \right) + \frac{\Delta G^\ddagger}{k_B T} \left(1 - \left(Z^2 - \frac{\nu F_{\text{eq}} x^\ddagger Z}{\Delta G^\ddagger} \right)^{\frac{1}{\nu}} \right) \right) \right) \right)^\nu \quad (\text{C6})$$

Using the approximation from Eq. (A6) in Eq. (C6) we will get Eq. (C7).

$$\langle F \rangle \approx \frac{\Delta G^\ddagger}{\nu x^\ddagger Z} \left(Z^2 - \left(1 - \frac{k_B T}{\Delta G^\ddagger} \ln \left(e^{\frac{\Delta G^\ddagger}{k_B T} \left(1 - \left(Z^2 - \frac{\nu F_{\text{eq}} x^\ddagger Z}{\Delta G^\ddagger} \right)^{\frac{1}{\nu}}} \right)} + \frac{x^\ddagger \dot{F} Z e^{-\gamma}}{k_0 k_B T} \right) \right) \right)^\nu \quad (\text{C7})$$

Next, we find the critical loading rate in the same way as in Appendix A.

$$1 - \frac{k_B T}{\Delta G^\ddagger} \ln \left(e^{\frac{\Delta G^\ddagger}{k_B T} \left(1 - \left(Z^2 - \frac{\nu F_{\text{eq}} x^\ddagger Z}{\Delta G^\ddagger} \right)^{\frac{1}{\nu}} \right)} + \frac{x^\ddagger \dot{F} Z e^{-\gamma}}{k_0 k_B T} \right) = 0$$

$$\dot{F} = \frac{k_0 k_B T e^{\frac{\Delta G^\ddagger}{k_B T} + \gamma}}{x^\ddagger Z} \left(1 - e^{-\frac{\Delta G^\ddagger}{k_B T} \left(Z^2 - \frac{\nu F_{\text{eq}} x^\ddagger Z}{\Delta G^\ddagger} \right)^{\frac{1}{\nu}}} \right)$$

By combining the two dependences that are valid for the different loading rate regimes as was done in Appendix A, using the Heaviside step function we obtain Eq. (C8).

$$\langle F_{\text{Rev}} \rangle \approx \frac{\Delta G^\ddagger}{\nu x^\ddagger Z} \left(Z^2 - \left| 1 - \frac{k_B T}{\Delta G^\ddagger} \left(e^{\frac{k_0 k_B T}{x^\ddagger \dot{F} Z} e^{\frac{\Delta G^\ddagger}{k_B T} \left(1 - \left(Z^2 - \frac{\nu F_{\text{eq}} x^\ddagger Z}{\Delta G^\ddagger} \right)^{\frac{1}{\nu}}} \right)}} E_1 \left(\frac{k_0 k_B T}{x^\ddagger \dot{F} Z} e^{\frac{\Delta G^\ddagger}{k_B T} \left(1 - \left(Z^2 - \frac{\nu F_{\text{eq}} x^\ddagger Z}{\Delta G^\ddagger} \right)^{\frac{1}{\nu}}} \right)} \right) + \frac{\Delta G^\ddagger}{k_B T} \left(1 - \left(Z^2 - \frac{\nu F_{\text{eq}} x^\ddagger Z}{\Delta G^\ddagger} \right)^{\frac{1}{\nu}} \right) \right) \right)^\nu \right).$$

$$\theta \left(\dot{F}_{\text{cRev}} - \dot{F} \right) + \left(\frac{\Delta G^\ddagger Z}{\nu x^\ddagger} - \sqrt{2 \dot{F}_{\text{cRev}} x^\ddagger \zeta} + \sqrt{2 \dot{F} x^\ddagger \zeta} \right) \cdot \theta \left(\dot{F} - \dot{F}_{\text{cRev}} \right) \quad (\text{C8})$$

$$\text{Where } \dot{F}_{\text{cRev}} = \frac{k_0 k_B T e^{\frac{\Delta G^\ddagger}{k_B T} + \gamma}}{x^\ddagger Z} \left(1 - e^{-\frac{\Delta G^\ddagger}{k_B T} \left(Z^2 - \frac{\nu F_{\text{eq}} x^\ddagger Z}{\Delta G^\ddagger} \right)^{\frac{1}{\nu}}} \right)$$

Eq. (C8) can be further simplified to Eq. (18) or using the approximation from Eq. (A6) to a similar equation to Eq. (A10).

Mean first unfolding force dependence on the loading rate for the unified model when the force is applied through spring

The mean first unfolding force dependence on the loading rate Eq. (17) can be obtained by starting the integration in Eq. (C3) from 0 and following the same steps, or by directly setting $F_{\text{eq}} = 0$ in Eq. (C8) and further simplifying.

Mean last unfolding force dependence on the loading rate for the unified model when the force is applied through spring

The mean first refolding force Eq. (19) and the mean reversible refolding force Eq. (20) that are used for calculating the mean last unfolding force when the force is applied through spring in Eq. (13), can be obtained using the same methods as described above, though using Eq. (C9) for the refolding rate (37) and limits of integration for $\langle F_{\text{FirstRef}} \rangle$ from F_{fin} to F in Eq. (C11) and for $\langle F_{\text{RevRef}} \rangle$ from F_{eq} to F in a similar equation.

$$k_{\text{ref}}(F) = k_{0\text{ref}} \left(Z_{\text{ref}}^2 + \frac{\nu F x_{\text{ref}}^{\ddagger} Z_{\text{ref}}}{\Delta G_{\text{ref}}^{\ddagger}} \right)^{\frac{1}{\nu}-1} e^{\frac{\Delta G_{\text{ref}}^{\ddagger}}{k_{\text{B}}T} \left(1 - \left(Z_{\text{ref}}^2 + \frac{\nu F x_{\text{ref}}^{\ddagger} Z_{\text{ref}}}{\Delta G_{\text{ref}}^{\ddagger}} \right)^{\frac{1}{\nu}} \right)} \quad (\text{C9})$$

$$\int k_{\text{ref}}(F) dF = -\frac{k_{0\text{ref}} k_{\text{B}} T}{x_{\text{ref}}^{\ddagger} Z_{\text{ref}}} e^{\frac{\Delta G_{\text{ref}}^{\ddagger}}{k_{\text{B}}T} \left(1 - \left(Z_{\text{ref}}^2 + \frac{\nu F x_{\text{ref}}^{\ddagger} Z_{\text{ref}}}{\Delta G_{\text{ref}}^{\ddagger}} \right)^{\frac{1}{\nu}} \right)} \quad (\text{C10})$$

Using Eq. (C10) in Eq. (C11) we get Eq. (C12).

$$\int_1^p \frac{dp'}{p'} = \frac{1}{F} \int_{F_{\text{fin}}}^F k_{\text{ref}}(F') dF' \quad (\text{C11})$$

$$\ln p = -\frac{k_{0\text{ref}} k_{\text{B}} T}{x_{\text{ref}}^{\ddagger} F Z_{\text{ref}}} \left(e^{\frac{\Delta G_{\text{ref}}^{\ddagger}}{k_{\text{B}}T} \left(1 - \left(Z_{\text{ref}}^2 + \frac{\nu F x_{\text{ref}}^{\ddagger} Z_{\text{ref}}}{\Delta G_{\text{ref}}^{\ddagger}} \right)^{\frac{1}{\nu}} \right)} - e^{\frac{\Delta G_{\text{ref}}^{\ddagger}}{k_{\text{B}}T} \left(1 - \left(Z_{\text{ref}}^2 + \frac{\nu F_{\text{fin}} x_{\text{ref}}^{\ddagger} Z_{\text{ref}}}{\Delta G_{\text{ref}}^{\ddagger}} \right)^{\frac{1}{\nu}} \right)} \right) \quad (\text{C12})$$

By solving Eq. (C12) for F we find Eq. (C13).

$$F = \frac{\Delta G_{\text{ref}}^{\ddagger}}{\nu x_{\text{ref}}^{\ddagger} Z_{\text{ref}}} \left(\left(1 - \frac{k_{\text{B}} T}{\Delta G_{\text{ref}}^{\ddagger}} \ln \left(e^{\frac{\Delta G_{\text{ref}}^{\ddagger}}{k_{\text{B}} T} \left(1 - \left(Z_{\text{ref}}^2 + \frac{\nu F_{\text{fin}} x_{\text{ref}}^{\ddagger} Z_{\text{ref}}}{\Delta G_{\text{ref}}^{\ddagger}} \right)^{\frac{1}{\nu}} \right)} - \frac{x_{\text{ref}}^{\ddagger} \dot{F} Z_{\text{ref}} \ln p}{k_{0\text{ref}} k_{\text{B}} T} \right) \right)^{\nu} - Z_{\text{ref}}^2 \right) \quad (\text{C13})$$

At this step, we follow the approximate averaging procedure as in (22).

$$\alpha \equiv \ln \left(e^{\frac{\Delta G_{\text{ref}}^{\ddagger}}{k_{\text{B}} T} \left(1 - \left(Z_{\text{ref}}^2 + \frac{\nu F_{\text{fin}} x_{\text{ref}}^{\ddagger} Z_{\text{ref}}}{\Delta G_{\text{ref}}^{\ddagger}} \right)^{\frac{1}{\nu}} \right)} - \frac{x_{\text{ref}}^{\ddagger} \dot{F} Z_{\text{ref}} \ln p}{k_{0\text{ref}} k_{\text{B}} T}} \right)$$

$$\langle F \rangle \approx F(\langle \alpha \rangle)$$

From Eq. (C13) and Eq. (A6) we will obtain for the mean first refolding force the Eq. (C14).

$$\langle F_{\text{FirstRef}} \rangle \approx \frac{\Delta G_{\text{ref}}^{\ddagger}}{\nu x_{\text{ref}}^{\ddagger} Z_{\text{ref}}} \left(\left(1 - \frac{k_{\text{B}} T}{\Delta G_{\text{ref}}^{\ddagger}} \left(e^{\frac{k_{0\text{ref}} k_{\text{B}} T}{x_{\text{ref}}^{\ddagger} \dot{F} Z_{\text{ref}}} e^{\frac{\Delta G_{\text{ref}}^{\ddagger}}{k_{\text{B}} T} \left(1 - \left(Z_{\text{ref}}^2 + \frac{\nu F_{\text{fin}} x_{\text{ref}}^{\ddagger} Z_{\text{ref}}}{\Delta G_{\text{ref}}^{\ddagger}} \right)^{\frac{1}{\nu}} \right)}} E_1 \left(\frac{k_{0\text{ref}} k_{\text{B}} T}{x_{\text{ref}}^{\ddagger} \dot{F} Z_{\text{ref}}} e^{\frac{\Delta G_{\text{ref}}^{\ddagger}}{k_{\text{B}} T} \left(1 - \left(Z_{\text{ref}}^2 + \frac{\nu F_{\text{fin}} x_{\text{ref}}^{\ddagger} Z_{\text{ref}}}{\Delta G_{\text{ref}}^{\ddagger}} \right)^{\frac{1}{\nu}} \right)}} \right) + \frac{\Delta G_{\text{ref}}^{\ddagger}}{k_{\text{B}} T} \left(1 - \left(Z_{\text{ref}}^2 + \frac{\nu F_{\text{fin}} x_{\text{ref}}^{\ddagger} Z_{\text{ref}}}{\Delta G_{\text{ref}}^{\ddagger}} \right)^{\frac{1}{\nu}} \right) \right) \right)^{\nu} - Z_{\text{ref}}^2 \right) \quad (\text{C14})$$

Using the approximation from Eq. (A6) in Eq. (C14) we will get Eq. (C15).

$$\langle F_{\text{FirstRef}} \rangle \approx \frac{\Delta G_{\text{ref}}^{\ddagger}}{\nu x_{\text{ref}}^{\ddagger} Z_{\text{ref}}} \left(\left(1 - \frac{k_{\text{B}} T}{\Delta G_{\text{ref}}^{\ddagger}} \ln \left(e^{\frac{\Delta G_{\text{ref}}^{\ddagger}}{k_{\text{B}} T} \left(1 - \left(Z_{\text{ref}}^2 + \frac{\nu F_{\text{fin}} x_{\text{ref}}^{\ddagger} Z_{\text{ref}}}{\Delta G_{\text{ref}}^{\ddagger}} \right)^{\frac{1}{\nu}} \right)} + \frac{x_{\text{ref}}^{\ddagger} \dot{F} Z_{\text{ref}} e^{-\gamma}}{k_{0\text{ref}} k_{\text{B}} T} \right) \right)^{\nu} - Z_{\text{ref}}^2 \right) \quad (\text{C15})$$

Next, we find the critical loading rate in the same way as previously.

$$1 - \frac{k_B T}{\Delta G_{\text{ref}}^{\ddagger}} \ln \left(e^{\frac{\Delta G_{\text{ref}}^{\ddagger}}{k_B T} \left(1 - \left(Z_{\text{ref}}^2 + \frac{\nu F_{\text{fin}} x_{\text{ref}}^{\ddagger} Z_{\text{ref}}}{\Delta G_{\text{ref}}^{\ddagger}} \right)^{\frac{1}{\nu}} \right)} + \frac{x_{\text{ref}}^{\ddagger} \dot{F} Z_{\text{ref}} e^{-\gamma}}{k_{0\text{ref}} k_B T} \right) = 0$$

$$\dot{F} = \frac{k_{0\text{ref}} k_B T e^{\frac{\Delta G_{\text{ref}}^{\ddagger}}{k_B T} + \gamma}}{x_{\text{ref}}^{\ddagger} Z_{\text{ref}}} \left(1 - e^{-\frac{\Delta G_{\text{ref}}^{\ddagger}}{k_B T} \left(Z_{\text{ref}}^2 + \frac{\nu F_{\text{fin}} x_{\text{ref}}^{\ddagger} Z_{\text{ref}}}{\Delta G_{\text{ref}}^{\ddagger}} \right)^{\frac{1}{\nu}}} \right)$$

By combining the two dependences that are valid for the different loading rate regimes as previously using the Heaviside step function we obtain Eq. (C16).

$$\langle F_{\text{FirstRef}} \rangle \approx \frac{\Delta G_{\text{ref}}^{\ddagger}}{\nu x_{\text{ref}}^{\ddagger} Z_{\text{ref}}} \left(\left(1 - \frac{k_B T}{\Delta G_{\text{ref}}^{\ddagger}} e^{\frac{k_{0\text{ref}} k_B T}{x_{\text{ref}}^{\ddagger} \dot{F} Z_{\text{ref}}} e^{\frac{\Delta G_{\text{ref}}^{\ddagger}}{k_B T} \left(1 - \left(Z_{\text{ref}}^2 + \frac{\nu F_{\text{fin}} x_{\text{ref}}^{\ddagger} Z_{\text{ref}}}{\Delta G_{\text{ref}}^{\ddagger}} \right)^{\frac{1}{\nu}} \right)}} \right) E_1 \left(\frac{k_{0\text{ref}} k_B T}{x_{\text{ref}}^{\ddagger} \dot{F} Z_{\text{ref}}} e^{\frac{\Delta G_{\text{ref}}^{\ddagger}}{k_B T} \left(1 - \left(Z_{\text{ref}}^2 + \frac{\nu F_{\text{fin}} x_{\text{ref}}^{\ddagger} Z_{\text{ref}}}{\Delta G_{\text{ref}}^{\ddagger}} \right)^{\frac{1}{\nu}} \right)} \right) + \frac{\Delta G_{\text{ref}}^{\ddagger}}{k_B T} \left(1 - \left(Z_{\text{ref}}^2 + \frac{\nu F_{\text{fin}} x_{\text{ref}}^{\ddagger} Z_{\text{ref}}}{\Delta G_{\text{ref}}^{\ddagger}} \right)^{\frac{1}{\nu}} \right) \right)^{\nu} - Z_{\text{ref}}^2 \right) \cdot \theta \left(\dot{F}_{\text{cFirst}} - \dot{F} \right) + \left(-\frac{\Delta G_{\text{ref}}^{\ddagger} Z_{\text{ref}}}{\nu x_{\text{ref}}^{\ddagger}} + \sqrt{2 \dot{F}_{\text{cFirst}} x_{\text{ref}}^{\ddagger} \zeta} - \sqrt{2 \dot{F} x_{\text{ref}}^{\ddagger} \zeta} \right) \cdot \theta \left(\dot{F} - \dot{F}_{\text{cFirst}} \right) \quad (\text{C16})$$

$$\text{Where } \dot{F}_{\text{cFirst}} = \frac{k_{0\text{ref}} k_B T e^{\frac{\Delta G_{\text{ref}}^{\ddagger}}{k_B T} + \gamma}}{x_{\text{ref}}^{\ddagger} Z_{\text{ref}}} \left(1 - e^{-\frac{\Delta G_{\text{ref}}^{\ddagger}}{k_B T} \left(Z_{\text{ref}}^2 + \frac{\nu F_{\text{fin}} x_{\text{ref}}^{\ddagger} Z_{\text{ref}}}{\Delta G_{\text{ref}}^{\ddagger}} \right)^{\frac{1}{\nu}}} \right).$$

Eq. (C16) can be further simplified to Eq. (19) or using the approximation from Eq. (A6) to a similar equation to Eq. (A10).

The mean reversible refolding force dependence on the loading rate when the force is applied through spring Eq. (20) can be obtained by starting the integration in Eq. (C11) from F_{eq} and following the same steps, or by directly setting F_{fin} to F_{eq} in Eq. (C16) and further simplifying.

References

1. Merkel R, Nassoy P, Leung A, Ritchie K, Evans E (1999) Energy landscapes of receptor–ligand bonds explored with dynamic force spectroscopy. *Nature* 397(6714):50–53.
2. Noy A (2011) Force spectroscopy 101: how to design, perform, and analyze an AFM-based single molecule force spectroscopy experiment. *Curr Opin Chem Biol* 15(5):710–718.
3. Noy A, Friddle RW (2013) Practical single molecule force spectroscopy: How to determine fundamental thermodynamic parameters of intermolecular bonds with an atomic force microscope. *Methods* 60(2):142–150.
4. Arya G (2016) Models for recovering the energy landscape of conformational transitions from single-molecule pulling experiments. *Mol Simul* 42(13):1102–1115.
5. Evans E, Ritchie K (1997) Dynamic strength of molecular adhesion bonds. *Biophys J* 72(4):1541–1555.
6. Busse WF, Lessig ET, Loughborough DL, Larrick L (1942) Fatigue of Fabrics. *J Appl Phys* 13(11):715–724.
7. Regel' VR, Slutsker AI, Tomashevskii ÉE (1974) *The kinetic nature of the strength of solids* (Nauka, Moscow).
8. Bell G (1978) Models for the specific adhesion of cells to cells. *Science* 200(4342):618–627.
9. Gergely C, et al. (2000) Unbinding process of adsorbed proteins under external stress studied by atomic force microscopy spectroscopy. *Proc Natl Acad Sci* 97(20):10802–10807.
10. Abramowitz M, Stegun IA (1972) *Handbook of Mathematical Functions With Formulas, Graphs and Mathematical Tables* (National Bureau of Standards, Washington D. C.).
11. Weisstein EW (2002) *CRC Concise Encyclopedia of Mathematics* (CRC Press, Boca Raton).
12. Zocher M, Zhang C, Rasmussen SGF, Kobilka BK, Muller DJ (2012) Cholesterol increases kinetic, energetic, and mechanical stability of the human 2-adrenergic receptor. *Proc Natl Acad Sci* 109(50):E3463–E3472.
13. Rico F, Russek A, González L, Grubmüller H, Scheuring S (2019) Heterogeneous and rate-dependent streptavidin–biotin unbinding revealed by high-speed force spectroscopy and atomistic simulations. *Proc Natl Acad Sci* 116(14):6594–6601.

14. Hummer G, Szabo A (2003) Kinetics from Nonequilibrium Single-Molecule Pulling Experiments. *Biophys J* 85(1):5–15.
15. Dudko O, Hummer G, Szabo A (2006) Intrinsic Rates and Activation Free Energies from Single-Molecule Pulling Experiments. *Phys Rev Lett* 96(10). doi:10.1103/PhysRevLett.96.108101.
16. Greenleaf WJ, Frieda KL, Foster DAN, Woodside MT, Block SM (2008) Direct Observation of Hierarchical Folding in Single Riboswitch Aptamers. *Science* 319(5863):630–633.
17. Yu H, et al. (2012) Energy landscape analysis of native folding of the prion protein yields the diffusion constant, transition path time, and rates. *Proc Natl Acad Sci* 109(36):14452–14457.
18. Bullerjahn JT, Sturm S, Kroy K (2014) Theory of rapid force spectroscopy. *Nat Commun* 5(1). doi:10.1038/ncomms5463.
19. Makarov DE (2016) Perspective: Mechanochemistry of biological and synthetic molecules. *J Chem Phys* 144(3):030901.
20. Kramers HA (1940) Brownian motion in a field of force and the diffusion model of chemical reactions. *Physica* 7(4):284–304.
21. Hänggi P, Talkner P, Borkovec M (1990) Reaction-rate theory: fifty years after Kramers. *Rev Mod Phys* 62(2):251–341.
22. Friddle RW (2008) Unified Model of Dynamic Forced Barrier Crossing in Single Molecules. *Phys Rev Lett* 100(13). doi:10.1103/PhysRevLett.100.138302.
23. Cossio P, Hummer G, Szabo A (2016) Kinetic Ductility and Force-Spike Resistance of Proteins from Single-Molecule Force Spectroscopy. *Biophys J* 111(4):832–840.
24. Chung HS, Eaton WA (2013) Single-molecule fluorescence probes dynamics of barrier crossing. *Nature* 502(7473):685–688.
25. Manosas M, Ritort F (2005) Thermodynamic and Kinetic Aspects of RNA Pulling Experiments. *Biophys J* 88(5):3224–3242.
26. Mossa A, Manosas M, Forns N, Huguët JM, Ritort F (2009) Dynamic force spectroscopy of DNA hairpins: I. Force kinetics and free energy landscapes. *J Stat Mech Theory Exp* 2009(02):P02060.
27. Manosas M, Mossa A, Forns N, Huguët JM, Ritort F (2009) Dynamic force spectroscopy of DNA hairpins: II. Irreversibility and dissipation. *J Stat Mech Theory Exp* 2009(02):P02061.
28. Junker JP, Ziegler F, Rief M (2009) Ligand-Dependent Equilibrium Fluctuations of Single Calmodulin Molecules. *Science* 323(5914):633–637.

29. Yu H, Siewny MGW, Edwards DT, Sanders AW, Perkins TT (2017) Hidden dynamics in the unfolding of individual bacteriorhodopsin proteins. *Science* 355(6328):945–950.
30. Ma L, et al. (2017) Single-molecule force spectroscopy of protein-membrane interactions. *eLife* 6:e30493.
31. Jiao J, et al. (2018) Munc18-1 catalyzes neuronal SNARE assembly by templating SNARE association. *eLife* 7:e41771.
32. Evans E (2001) Probing the Relation Between Force—Lifetime—and Chemistry in Single Molecular Bonds. *Annu Rev Biophys Biomol Struct* 30(1):105–128.
33. Friddle RW, Noy A, De Yoreo JJ (2012) Interpreting the widespread nonlinear force spectra of intermolecular bonds. *Proc Natl Acad Sci* 109(34):13573–13578.
34. Friddle RW (2016) Analytic descriptions of stochastic bistable systems under force ramp. *Phys Rev E* 93(5). doi:10.1103/PhysRevE.93.052126.
35. Maitra A, Arya G (2010) Model Accounting for the Effects of Pulling-Device Stiffness in the Analyses of Single-Molecule Force Measurements. *Phys Rev Lett* 104(10). doi:10.1103/PhysRevLett.104.108301.
36. Hinczewski M, Hyeon C, Thirumalai D (2016) Directly measuring single-molecule heterogeneity using force spectroscopy. *Proc Natl Acad Sci* 113(27):E3852–E3861.
37. Pierse CA, Dudko OK (2013) Kinetics and Energetics of Biomolecular Folding and Binding. *Biophys J* 105(9):L19–L22.
38. Alsteens D, et al. (2015) Imaging G protein–coupled receptors while quantifying their ligand-binding free-energy landscape. *Nat Methods* 12(9):845–851.
39. Alsteens D, et al. (2016) Nanomechanical mapping of first binding steps of a virus to animal cells. *Nat Nanotechnol* 12(2):177–183.
40. Reiter-Scherer V, et al. (2019) Force Spectroscopy Shows Dynamic Binding of Influenza Hemagglutinin and Neuraminidase to Sialic Acid. *Biophys J* 116(6):1037–1048.
41. Petrosyan R, et al. (2015) Single-Molecule Force Spectroscopy of Membrane Proteins from Membranes Freely Spanning Across Nanoscopic Pores. *Nano Lett* 15(5):3624–3633.
42. Yu H, Heenan PR, Edwards DT, Uyetake L, Perkins TT (2019) Quantifying the Initial Unfolding of Bacteriorhodopsin Reveals Retinal Stabilization. *Angew Chem* 131(6):1724–1727.
43. Neupane K, et al. (2016) Direct observation of transition paths during the folding of proteins and nucleic acids. *Science* 352(6282):239–242.

44. Schulten K, Kosztin I (2000) *Lectures in Theoretical Biophysics* (University of Illinois at Urbana–Champaign, Urbana IL).
45. Szabo A, Schulten K, Schulten Z (1980) First passage time approach to diffusion controlled reactions. *J Chem Phys* 72(8):4350–4357.
46. Reimann P, Schmid GJ, Hänggi P (1999) Universal equivalence of mean first-passage time and Kramers rate. *Phys Rev E* 60(1):R1–R4.
47. Hyeon C, Thirumalai D (2007) Measuring the energy landscape roughness and the transition state location of biomolecules using single molecule mechanical unfolding experiments. *J Phys Condens Matter* 19(11):113101.
48. Tshiprut Z, Urbakh M (2009) Exploring hysteresis and energy dissipation in single-molecule force spectroscopy. *J Chem Phys* 130(8):084703.